Exploration of glass domain in the SiO2-B2O3-La2O3 system

H. Trégouët, D. Caurant, O. Majerus, T. Charpentier, T. Lerouge, L. Cormier

Exploration of glass domain in the SiO_2-B_2O_3-La_2O_3 system

H. Trégouët,[a] D. Caurant,[a,*] O. Majérus,[a] T. Charpentier,[b] T. Lerouge[a] and L. Cormier[c]

[a] *Chimie ParisTech, PSL Research University, CNRS, Institut de Recherche de Chimie Paris (IRCP), UMR 8247, 11, rue Pierre et Marie Curie, 75005, Paris, France*

[b] *NIMBE, CEA, CNRS, Université Paris-Saclay, 91191 Gif-sur-Yvette, France*

[c] *Institut de Minéralogie, de Physique des Matériaux, et de Cosmochimie (IMPMC), Sorbonne Universités-UPMC Université Paris 06, CNRS UMR 7590, 75005, Paris, France*

ABSTRACT

The existence of a relatively wide glass domain has been put in evidence in the SiO_2-B_2O_3-La_2O_3 ternary system, using a melt-quenching method. This domain extends from a region surrounding the lanthanum metaborate (LaB_3O_6) composition in the B_2O_3-La_2O_3 binary system to ternary compositions bearing up to 39 mol% SiO_2. Outside this domain, phase separation phenomena and/or crystallization of La-rich borate ($LaBO_3$) and borosilicate ($La_3Si_2BO_{10}$) phases are observed during quenching. The evolution of glass transition temperature (T_g) with composition in the glassy domain has been studied and discussed according to structural changes put in evidence by ^{11}B MAS NMR. Moreover, the evolution of the thermal stability of a series of glasses derived from a lanthanum metaborate glass by substituting B_2O_3 by increasing amount of SiO_2 (up to 36 mol% SiO_2) was studied by DTA and thermal treatments followed by characterization by XRD and Raman spectroscopy. In spite of silica-enrichment along the glass series, the first phases crystallizing during heating were always lanthanum borates (LaB_3O_6, $LaBO_3$) according the following sequence when SiO_2 content increases:

* Corresponding author. E-mail address: daniel.caurant@chimie-paristech.fr (D. Caurant)

$LaB_3O_6 \rightarrow LaB_3O_6 + LaBO_3\text{-LT} \rightarrow LaBO_3\text{-LT} \rightarrow LaBO_3\text{-LT} + LaBO_3\text{-HT}$ (LT and HT for low and high temperature forms respectively). The evolution of the nature of crystalline phases and thermal stability is discussed taking into account the changes occurring in glass structure with SiO_2 content. Because of their high glass transition temperature (T_g > 660°C) and their lack of hygroscopicity, transparent glasses in this system could find application, for instance in optics by partially substituting La by optically active rare earths.

1. Introduction

Due to their low thermal expansion and high chemical durability, borosilicate glasses represent an important subject of interest as they are encountered in many fields, such as laboratory glassware, cookware, drug packaging, optics, lighting and flat-panel display. Borosilicate glass matrices are also used widely to immobilize highly radioactive nuclear waste, because they provide high incorporation capacity, good thermal stability and long-term chemical durability and self-irradiation resistance [1]. Such nuclear waste glasses are very complex systems, bearing numerous chemical elements and in particular, large amounts of rare earth (RE) elements originating from the fission processes that occur in the fuel during its stay in nuclear reactors. Indeed, REs represent one of the most abundant families of elements present in the solutions arising from spent fuel reprocessing (about 20 wt% RE oxides) [2].

Previous studies on a RE-rich 7-oxides borosilicate glass, used as a model for nuclear waste glass developed to immobilize high concentration of waste, showed that the incorporation of RE^{3+} ions was greatly impacted by variations of B_2O_3 content, which could be due to the existence of a structural relationship between RE and B in the glassy structure [3], while studies performed on other RE-rich borosilicate glasses suggest the formation of a local RE-metaborate structure incorporating preferentially RE^{3+} ions [4,5,6]. To improve the understanding of RE-rich borosilicate glasses structure and also to enhance the immobilization properties of nuclear

waste glasses, it is thus of great interest to elucidate the chemical and structural relationship that could exist between boron and RE in glasses, starting with the simplest systems bearing simultaneously these two oxides, like B_2O_3-RE_2O_3 binary system [7,8,9,10] or SiO_2-B_2O_3-RE_2O_3 ternary system, and then progressively increasing the complexity of the glass composition.

In this work, we focus our interest on RE = La because La is one of the most abundant RE in nuclear waste [2] and it enables to perform NMR characterization (La^{3+} ion is not paramagnetic). It appears that only few data have been gathered on the possibility to prepare glasses in the SiO_2-B_2O_3-La_2O_3 ternary system [11,12]. Moreover, to the best of our knowledge, no phase diagram has been reported in literature for this ternary system with La_2O_3 or any of the other RE oxides. Usually, another component, such as an alkali oxide, is added to the ternary system to facilitate glass preparation [13,14]. In comparison with the very little studied SiO_2-B_2O_3-RE_2O_3 ternary system, an important number of studies have been reported on glasses belonging to the SiO_2-Al_2O_3-RE_2O_3 ternary system containing aluminum in place of boron [15,16,17,18,19,20,21,22,23]. RE aluminosilicate glasses have been envisaged both for optical applications [16,18] and as matrices for the storage of actinides produced by nuclear industry [20,21].

In this paper, we will first outline bibliographic data on crystalline and glassy phases reported in the SiO_2-B_2O_3-La_2O_3 system. Then, we will present results concerning the extension of the glass domain in this system, obtained after melt quenching specifying the phases formed outside this domain. The effect of changing the composition of glasses belonging to this ternary system on their crystallization tendency during heating (thermal stability and nature of crystalline phases) will be also presented. The main objective of the present work is to bring elements of knowledge on this ternary system little studied in literature but involving compounds frequently used in more complex glasses (SiO_2, B_2O_3 and RE_2O_3) for instance for nuclear waste

immobilization or optical applications. Such ternary glasses could find applications in optics by partially replacing lanthanum by a trivalent optically active RE in their compositions. Moreover, the study of the evolution of their crystallization tendency and structure by changing composition may be useful to understand the thermal stability and structural characteristics of complex borosilicate nuclear glasses containing RE. A detailed structural study of the SiO_2-B_2O_3-La_2O_3 ternary glasses will be presented in another paper. The crystallization and structural study of the RE-metaborate (REB_3O_6) glass composition belonging to the B_2O_3-RE_2O_3 binary system for RE = La and Nd was already published [9,10,24].

2. Crystalline and glassy phases in SiO_2-B_2O_3-La_2O_3 ternary system

2.1. Crystalline phases

Ten crystalline phases belonging to the SiO_2-B_2O_3-La_2O_3 ternary system have been reported in the literature: three phases in the B_2O_3-La_2O_3 binary system (La_3BO_6, $LaBO_3$ and LaB_3O_6) [25] three phases in the SiO_2-La_2O_3 binary system (La_2SiO_5, $La_{9.33}Si_6O_{26}$ and $La_2Si_2O_7$) [26,27,28], and four phases bearing simultaneously SiO_2, B_2O_3 and La_2O_3 ($LaBSiO_5$, $La_3Si_2BO_{10}$, $La_{9.66}Si_5BO_{26}$ and $La_{10}Si_4B_2O_{26}$) on which closer attention will be paid below. However, no crystalline phases containing both SiO_2 and B_2O_3 have been reported in the SiO_2-B_2O_3 binary system [29]. According to the crystallization results that will be presented below, it is important to note that two forms have been reported in the literature for $LaBO_3$ (La-orthoborate): a high-temperature form (HT) and a low-temperature form (LT) that all consist of isolated BO_3 units ($(BO_3)^{3-}$) bearing three non-bridging oxygen atoms (NBOs) [30,31,32]. All the crystalline phases reported in literature are indicated in the SiO_2-B_2O_3-La_2O_3 ternary diagram shown in Fig. 1.

Stillwellite $REBSiO_5$ ($RE_2O_3.B_2O_3.2SiO_2$) was first discovered in an Australian ore deposit [33], with major RE being Ce, and has since been synthesized and studied for different REs (La, Ce, Pr, Nd, Sm) [34,35], using either solid-state reaction or hydrothermal synthesis. The crystalline structure belongs to the trigonal crystal system (space group $P3_1$) [36,37]. It is composed of infinite helical chains of BO_4 and SiO_4 units (Fig. 2a). Si atoms, bearing two NBOs, are linked to two consecutive BO_4 units (which do not bear any NBOs) by two bridging oxygen atoms (BOs), thus forming 6-membered rings (1Si + 2B + 3O) linked by the BO_4 units along the 3_1 axis [38]. It is important to underline that no BO_3 units exist in this structure. RE^{3+} ions are located along an axis formed by the Si atoms. They are surrounded by nine oxygen atoms [38] (Table 1): 4 NBOs linked to Si atoms, 4 BOs engaged in Si-O-B bonds and 1 BO engaged in a B-O-B bond. It is worth noting here the similarities between the crystalline structure of stillwellite $LaBSiO_5$ ($La_2O_3.B_2O_3.2SiO_2$) and La-metaborate LaB_3O_6 ($La_2O_3.3B_2O_3$). Transforming LaB_3O_6 into $LaBSiO_5$ is equivalent to replacing $2B_2O_3$ by $2SiO_2$ i.e. transforming $[B_3O_6]^{3-}$ units into $[BSiO_5]^{3-}$ units. LaB_3O_6 is formed of infinite chains of 8-membered rings ($2BO_4 + 2BO_3$) linked by the BO_4 units, analogous to the stillwellite infinite chains [39]. For temperature above 140°C (for RE = La), a phase transition of stillwellite toward a monoclinic structure (space group $P3_121$) is observed, leading to a slight distortion of the structure but maintaining the helical chains of rings [40,41]. Stillwellite is of interest because of its ferroelectric, non-linear optical and piezoelectric properties [42,43]. This phase was also reported as a product formed during nuclear waste glass dissolution experiment under severe conditions [44]. For RE = Gd, a distinct phase exhibiting the same stoichiometry as stillwellite ($GdBSiO_5$) and belonging to the monoclinic crystal system was observed, identical to the one reported for small REs (Nd-Dy) within the $REBGeO_5$ (borogermanate) family [35,45]. Otherwise, for bigger RE (La-Nd), $REBGeO_5$ exhibits the same crystalline structure as stillwellite, along with ferroelectric properties [35,45].

The existence of the RE borogermanosilicate $RE_3Ge_{1.08}Si_{0.92}BO_{10}$ crystalline phase was first reported [46] and then synthesized with Si atoms only, which led to $RE_3Si_2BO_{10}$ ($3RE_2O_3.B_2O_3.4SiO_2$) composition with RE = Sm [47], Eu [48], Ce [49], Nd [50], La [51], Gd [51] and Dy [51]. This crystalline structure is orthorhombic (space group Pbca) [46] and exhibits alternating layers of $(SiO_4)^{4-}$ (Q_0 units) and $(BSiO_6)^{5-}$ entities, along the c axis (Fig. 2b). $(BSiO_6)^{5-}$ groups consist in a BO_3 triangle ($B\O O_2^{2-}$ where Ø is a bridging oxygen atom) linked to a SiO_4 tetrahedron by one oxygen atom (Q_1 unit). There are no BO_4 units in this structure and only Si-O-B bonds are observed. $(BSiO_6)^{5-}$ groups are analogous to the $(Si_2O_7)^{6-}$ dimers observed in $La_2Si_2O_7$ [28]. RE^{3+} ions are located in three distinct sites, coordinated either to 8 or 9 oxygen atoms (Table 1). These crystals were first obtained while attempting to form other RE-rich crystalline phases, such as borovanadates or fluoride borates by reaction in a sealed quartz tube [47,49,50] (which led to a contamination of the melt by SiO_2), or were intentionally prepared either by solid-state reaction and chemical vapor transport methods [48] or from high temperature solutions [51]. Very recently, $Nd_3Si_2BO_{10}$ was reported as a product of crystallization in glass system simulating nuclear glass waste [52].

$RE_{10}Si_4B_2O_{26}$ oxyapatite crystals (RE = La [53,54], Y [54], Gd [54,55], Pr [55], Nd [55], Sm [55], Eu [55], Dy [55], Tb [56]) belong to the hexagonal crystal system (space group $P6_3/m$). The oxyapatite structure is common to $La_{9.66}Si_5BO_{26}$ and pure silicate $RE_{9.33}Si_6O_{26}$ compounds [27,28], with the replacement of one or two Si atoms by one or two B atoms thus creating negative charges which are compensated by 1/3 or $2/3RE^{3+}$ ions per formula unit. The structure consists in isolated $(SiO_4)^{4-}$ (Q^0 units) and $(BO_4)^{5-}$ units, along with free oxygen atoms O^{2-} (Fig. 2c.). It is important to note the presence of very charged boron tetrahedral $(BO_4)^{5-}$ units in the mixed B-Si apatite. To the best of our knowledge, this is the only occurrence of such isolated boron tetrahedral units in a crystalline structure. RE^{3+} ions are located in two different sites, either in 7-fold coordination (6h site) or 9-fold coordination (4f site). The 6h site is surrounded

by 1 free oxygen anion and 6 NBOs whereas the 4f site is coordinated by NBOs only. $RE_{10}Si_4B_2O_{26}$ crystals were obtained either via wet chemical route, flux or solid-state reaction. $RE_{10}Si_4B_2O_{26}$ with TR = Tm, Yb or Lu could not be formed (at least under the same wet chemical conditions) [54] due to the small size of RE^{3+} ions, and RE_2SiO_5 and $REBO_3$ phases were formed instead. $RE_{10}Si_4B_2O_{26}$ compounds represent good host lattices in order to prepare luminescent materials or possible magneto-optical materials [54,55,56,57]. $La_{9.66}Si_5BO_{26}$ is also an oxyapatite phase but to the best of our knowledge only one paper reported the existence of this phase [53]. In comparison with the oxyapatite $La_{10}Si_4B_2O_{26}$ described above, one B atom has been here substituted by one Si atom involving a positive charge excess compensated by the rejection of $0.33La^{3+}$ ions (i.e. one positive charge by formula unit).

2.2. Glassy phases

Following the discovery and study of crystalline stillwellite ($LaBSiO_5$)-like materials, several studies were carried out, dealing with the glass formation domain in the ternary system SiO_2-B_2O_3-La_2O_3, in order to prepare ferroelectric glass-ceramics with pyroelectric properties, by controlled crystallization of the glass [11,58]. In this case, several glass samples were obtained in a restricted domain of the ternary system close to the stillwellite composition (Fig. 1), by melting reagent mixtures between 1480 and 1550°C followed by rapid quenching between metallic plates. Some of these samples were reported as transparent according to the authors, like the one with the stillwellite stoichiometric composition. Nevertheless, it is important to underline that numerous samples prepared in these studies were melted in corundum crucibles which could induce melt pollution by Al_2O_3. However, the authors of these studies did not report any chemical analysis of their samples melted in such crucibles to check this point [11,58]. Different properties of these glasses were studied, such as density, dielectric permeability and dielectric loss [11]. Crystallization of three different phases were put in

evidence when performing heat treatment on the glassy samples: $LaBSiO_5$ (stillwellite), $LaBO_3$ (La-orthoborate) and $La_2Si_2O_7$, as single-phase or polyphase systems [11,58]. Structural changes between $LaBSiO_5$ glasses and glass-ceramics, such as loss of long-range ordering and its influence over the structural units like BO_4 units, were studied using infrared reflectivity and Raman spectroscopy [59], but not with NMR spectroscopy. More recently, some work focused on the electrodynamic characteristics of this kind of stillwellite-based materials, in relation with optical applications [60]. However, a higher number of studies has been performed on the analogous RE-borogermanate glasses [58,61,62,63] where SiO_2 was totally replaced by GeO_2 for various reasons according to the authors of these works: i) It is easier to vitrify ternary compositions when SiO_2 is replaced by GeO_2, ii) Ge-containing glass compositions show a better ability to crystallize in stillwellite ($REBGeO_5$) at low temperature than Si-containing glasses and finally iii) $LaBGeO_5$ crystals exhibit an interesting combination of properties, such as high electrical resistance and pyroelectric coefficient.

A recent study on high refractive-index glasses, related to the BaO-La_2O_3-B_2O_3-TiO_2-SiO_2 system, also started from the SiO_2-B_2O_3-La_2O_3 ternary system [12]. In comparison with the works performed on glasses with composition close to stillwellite presented above, a wider zone of the diagram was explored by these authors (Fig. 1), by heating their mixtures at lower temperature (1400°C) in Pt crucibles but they did not give any indication about their quenching method and rate. Depending on their composition, the samples obtained exhibited phenomena of partial or total crystallization or phase separation after melting or only sintering of the initial mixture without melting, or were completely homogeneous, transparent and XRD amorphous (Fig. 1). For instance, mixtures with high La_2O_3 content (40-60 mol%) did not lead to homogeneous melt and had a high tendency to crystallize, whereas mixtures with high B_2O_3 content (40-60 mol%) and 20-40 mol% SiO_2 lead to phase separation. However, mixtures with 20-30 mol% La_2O_3, 40-50 mol% SiO_2 and 30-60 mol% B_2O_3 lead to homogeneous glasses after

melting (Fig. 1) and the evolution of their viscosity with temperature was measured (as expected, SiO_2 substitution by B_2O_3 induced viscosity decrease). Moreover, these glasses exhibit refractive index between 1.63 and 1.72 and their linear thermal expansion coefficient (CLTE) varies in the range (60-70).10^{-7}°C^{-1}. Several structural characterizations were performed on homogeneous glasses by IR spectroscopy, indicating that the introduction of increasing La_2O_3 amount induced a decrease of the silicate network polymerization and an increase of the proportion of BO_3 units [12]. Once again, the authors did not report any NMR study of their glasses.

3. Experimental Procedures

3.1. Glass synthesis

In order to explore the glass domain in the ternary system SiO_2-B_2O_3-La_2O_3, numerous samples whose compositions are given in Tables 2-3 and in Fig. 3 (different series from Ax to Gx can be distinguished) were prepared starting with mixing reagent-grade powders of La_2O_3 (dried for 12 hours at 1000°C to remove any water trace), SiO_2 (dried for 12h at 400°C) and H_3BO_3. The mixture (10-30 g) was then placed in a platinum crucible, heated, under air, at 1550°C for 30 min and quenched by casting and pressing between brass plates (obtaining plates less than 1mm thick). According to a previous study using a similar melt quenching method [64], the quenching rate may be estimated close to 10^4°C/min. The short melting duration (30 min) was chosen to limit boron evaporation (B_2O_3 is the only volatile oxide in the mixture). Some compositions that easily vitrify were also cooled directly under air in the platinum crucible after removal from the furnace (natural cooling), this is the case for instance for the samples of the Ax series derived from the La-metaborate glass composition by substituting increasing SiO_2 amounts for B_2O_3 (Table 2, Fig. 3). Some quenched samples with composition close to stillwellite ($LaBSiO_5$) were ground, melted and pressed again, in order to try to obtain clear

glasses. Indeed, such compositions close to stillwellite were reported in literature as leading to transparent glasses [11], but we did not succeed in obtaining transparent samples despite several attempts also modifying the weight of mixture in the crucible, the melting temperature and duration, and even introducing slight B_2O_3 excess (several mol%) in the mixture to take into account a possible boron volatilization during melting. The composition of several samples (see Tables 2 and 3) was checked by EPMA (CAMPARIS, Paris, France) with a CAMECA SX100 apparatus (15 kV, 50 nA) using the following standard references: BN for boron, La_3ReO_8 for lanthanum and $CaMgSi_2O_6$ for silicon. It appeared that analyzed compositions were close to nominal compositions (never more than 5% of the initial B_2O_3 amount evaporates during melting). Thus, in the rest of this article, the actual glasses composition will be considered as similar to their theoretical composition.

In the present study, a sample is considered as glassy if it exhibits transparent and XRD amorphous areas of at least 1 cm^2 (Fig. 4a) after quenching of the melt by pressing between metallic plates or by natural cooling after crucible removal from the furnace (Fig. 4b). For several transparent XRD amorphous samples the absence of crystalline phases was verified by scanning electron microscopy (SEM). The presence of small phase separated or crystallized areas outside the transparent glassy area (Figs. 4c,e and 5c,e) may be due to less efficient quenching rate in the corresponding regions of the sample. The completely opaque and XRD amorphous samples (Fig. 4d) are reported as phase separated as verified by SEM (Fig. 5a), whereas the samples with small transparent areas (less than 1 cm^2) along with opaque XRD amorphous zones are marked as partially phase separated (Fig. 4c). When crystallization occurs in the entire sample, as put in evidence by SEM, XRD and Raman spectroscopy, the samples are reported as crystallized (Figs. 4f and 5f). The nominal compositions of all the samples prepared in this study are reported in Tables 2 and 3 and their state after quenching (glassy with or without phase separation, or crystallized) is indicated in the ternary diagram (Fig. 3).

To enable the identification by XRD and Raman spectroscopy of the crystalline phases formed in several samples during melt quenching, the following reference phases were prepared as ceramics by solid state reaction: $LaBO_3$ (LT and HT), $La_3Si_2BO_{10}$, $La_{10}Si_4B_2O_{26}$ and $LaBSiO_5$. For this, stoichiometric proportions of H_3BO_3, SiO_2 and La_2O_3 were weighted, mixed, pressed and sintered at different temperatures for different times: $LaBO_3$-LT (900°C-9h), $LaBO_3$-HT (1550°C-4h + 1580°C-2h + quenching in water), $La_3Si_2BO_{10}$ (950°C-12h + 1200°C-12h + 1550°C-72h), $La_{10}Si_4B_2O_{26}$ (950°C-12h + 1200°C-12h + 1500°C-12h), $LaBSiO_5$ (950°C-12h + 1200°C-12h + 1500°C-12h). According to the samples, intermediate grinding + sintering operations were carried out to improve the single-phase character of the ceramics. To complete this series, a LaB_3O_6 crystalline reference sample was prepared by crystallization (850°C-12h) of LaB_3O_6 glass. Except $LaBSiO_5$ sample that contains small amounts of $La_3Si_2BO_{10}$, all other samples exhibit good single-phase character (see Fig. 6 below).

3.2. Samples characterization

X-ray diffraction (XRD) powder measurements were carried out to check for the presence of crystalline phases in all quenched transparent and partially or totally opaque samples, with the help of an X'Pert PRO PANalytical instrument ($\lambda_{Cu\text{-}K\alpha}$ = 0.15406 nm) at room temperature. For comparison, the XRD patterns of the reference crystalline phases (ceramic samples) were also recorded. The microstructure (crystallization and phase separation) of the partially or totally opaque samples was studied with the help of a JEOL 7800F Field Emission Gun Scanning Electron Microscope (FEG-SEM), in back-scattered electron (BSE) mode coupled with EDX using a BRUKER Quantax 400 system.

Differential thermal analysis (DTA) measurements were performed on a DTA/TG STA 449 Netzsch apparatus, using powdered glass samples (~ 200 mg) with controlled grain size (80-125μm) and a heating rate of 10°C/min to determine the glass transition temperature T_g

(determined as the onset of the first endothermic effect) and to check the exothermic effects associated with crystallization. In order to get more information on glass thermal stability and on the crystallization processes occurring during heating, the glasses of the Ax series were heat-treated for 10 minutes at a temperature close to the extremum (T_p) of the first exothermic effect observed on their DTA curve and then studied by XRD and Raman spectroscopy. Raman spectra of partially crystallized samples and of reference crystalline phases were acquired at room temperature with the help of a Renishaw Invia apparatus with laser excitation at $\lambda = 473$ nm. Spectra were recorded on the 200-1500 cm^{-1} range in dispersive mode with a 2400 lines/mm grating and a CCD camera.

^{11}B MAS NMR (Magic Angle Spinning Nuclear Magnetic Resonance) study of three glass series (Ax, Bx and Dx) has been performed to follow the evolution with composition of the relative proportion of BO_3 and BO_4 units deduced from spectra simulation. Experiments were performed using a Bruker Avance II 500WB spectrometer, operating at a magnetic field of 11.72T (^{11}B Larmor frequency of 160.14 MHz). Spectra were collected at a sample spinning frequency of 12.5 or 14 kHz using a commercial CPMAS zirconia probe. Chemical shifts are reported in ppm relative to an external sample of 1 M aqueous boric acid (19.6 ppm). All spectra were processed and simulated to extract the relative proportions of BO_3 and BO_4 units according to a theoretical approach described elsewhere [65].

4. Results

4.1. Exploration of the glass domain

The glass formation domain (transparent glasses) that has been determined in this work (Fig. 3) extends from compositions belonging to the B_2O_3-La_2O_3 binary system close to the lanthanum metaborate composition (A0) to compositions in the ternary system that can contain more than 38 mol% SiO_2 (B4). This glass domain is marked out on the right side of the diagram

by a wide area roughly parallel to the join SiO_2-B_2O_3 where phase separation (without crystallization) occurs during melt quenching leading to opalescent or opaque glasses (Figs. 4c,d and 5a-d). This area corresponds to compositions that contain less than 18 mol% La_2O_3 near the join B_2O_3-La_2O_3 to compositions with less than 27.5 mol% La_2O_3 near stillwellite ($LaBSiO_5$). On the left side of the diagram, roughly parallel to the join SiO_2-B_2O_3, the glass domain is marked out by strong crystallization tendency ($LaBO_3$, $La_3Si_2BO_{10}$, $La_2Si_2O_7$) during melt quenching for samples bearing more than 35-40.5 mol% La_2O_3 (C6, F0-F2) (Figs. 4f and 5f). For slightly lower La_2O_3 content (Dx series), partial crystallization can be observed in limited regions of the samples that were probably not quenched as efficiently as the main transparent glassy regions (Figs. 4e and 5e). It can be noted that for the SiO_2-poor samples such as F0, the crystallization of the low temperature form of $LaBO_3$ ($LaBO_3$-LT) as main phase was observed by XRD (Fig. 6) and Raman spectroscopy (Fig. 7), whereas for samples with higher SiO_2 content such as F2 and S2, the crystallization of the high temperature form of $LaBO_3$ ($LaBO_3$-HT) at the same time as $La_3Si_2BO_{10}$ occurs (with sometimes small amounts of $La_2Si_2O_7$ and $LaBO_3$-LT) (Figs. 6 and 7). Due to the increasing crystallization tendency of the melt with La_2O_3 content and to the high refractory character of this oxide (mp = 2304°C) [66] in comparison with SiO_2 (mp = 1722°C) [66] and B_2O_3 (mp = 450°C) [66], we did not try to melt and quench compositions containing more than 40.5 mol% La_2O_3 (F1) that would have most certainly not led to transparent glasses. As for compositions with SiO_2 content of the order of 47-50 mol% only phase separated or crystallized samples were obtained (B5, E5), we did not try to melt and quench compositions with SiO_2 content higher than 50 mol%.

Concerning the SiO_2-B_2O_3 system that represents the right side of the triangular diagram (Fig. 3), in accordance with literature results [67] some of us verified in a previous paper [68] the possibility to easily obtain transparent glasses in this system without La_2O_3 in spite of the existence of a subliquidus miscibility gap [69]. Nevertheless, as it is the case for pure SiO_2 and

B_2O_3 [25,26] as soon as a small La_2O_3 amount is introduced in binary SiO_2-B_2O_3 compositions, a strong phase separation is put in evidence with formation of small amorphous droplets as shown in Fig. 5d (G1) when 1 mol% La_2O_3 was added to the $80SiO_2$-$20B_2O_3$ composition (G0) and homogeneous glasses cannot be obtained, which suggests the existence of a wide immiscibility gap all along the join SiO_2-B_2O_3 probably making the connection between the two binary immiscibility gaps (SiO_2-La_2O_3 and B_2O_3-La_2O_3). It is interesting to remark that, whereas for the phase separated samples (such as C3, C4, C14, E0) close to the main glass domain presented above, SEM and EDX show the presence of isolated or aggregated amorphous La-poor particles appearing in black on the BSE SEM images (Fig. 5b,c), the droplets appear in white on the BSE SEM image of sample G1 (Fig. 5d). This difference indicates a strong La-enrichment in the droplets for this sample in accordance with EPMA analysis ($36SiO_2$-$35B_2O_3$-$29La_2O_3$ in mol%). It can be noted that the composition of the droplets in sample G1 is the same as the one of glass A6 located in the ternary glass domain (Fig. 3) in accordance with the possible existence of a large immiscibility gap in the ternary system all along the join SiO_2-B_2O_3.

The extended glass series Ax almost parallel to the join B_2O_3-SiO_2 is well representative of the extent of the glass formation domain highlighted in Fig. 3, starting from the lanthanum metaborate (A0) composition to the $36SiO_2$-$35B_2O_3$-$29La_2O_3$ (A6) composition (by progressively substituting B_2O_3 by SiO_2). The Ax series was selected to follow the evolution of T_g and for the crystallization investigations presented below because this series very easily lead to totally transparent glass samples either by melt quenching between metallic plates or by natural cooling of the melt in the Pt crucible outside the furnace (Fig. 4b). The evolution of T_g for the transparent glass samples of the Dx series (roughly parallel to the Ax series but with higher La_2O_3 content (~ + 7.5 mol%)) and Bx series (with increasing B_2O_3 content (B1 to B4)) series is also presented below.

It is important to remark that any sign of hygroscopicity was not detected for none of the transparent glasses of the B_2O_3-La_2O_3 binary and SiO_2-B_2O_3-La_2O_3 ternary systems, in spite of the high B_2O_3 content of these glasses, which is very interesting for potential applications in the field of optics for instance. This observation is in agreement with that reported by Chakraborty et al. [7] for B_2O_3-La_2O_3 binary glasses.

4.2. Evolution of glass transformation temperature in the SiO_2-B_2O_3-La_2O_3 system

DTA experiments were carried out on a large number of glassy transparent samples and on the transparent areas of slightly crystallized samples. Values of glass transition temperature (T_g) are distributed between 666 and 712°C ± 2°C within the vitreous domain (Tables 2 and 3). T_g was also measured for the sample with stillwellite composition (E5) which exhibits phase separation (Figs. 4d and 5a), and the value obtained (716°C) is in accordance with the values given by Sigaev et al. [11] (710-720°C) for their glass samples with composition close to stillwellite. The evolution of T_g for Ax, Dx and Bx series is shown in Fig. 8a. For the Ax series, where B_2O_3 is progressively substituted by SiO_2, it appears that T_g remains almost constant (674-678°C) as long as SiO_2 content remains ≤ 18 mol% (A0-A3) and then significantly increases from 681 to 697°C (A4-A6) when SiO_2 content reaches 36 mol%. For glasses of the Dx series (D0-D4, containing about 7.5 mol% La_2O_3 more than glasses of the Ax series, Fig. 3), a continuous increase of T_g is observed when B_2O_3 is substituted by SiO_2 along the series from the binary glass D0 (666°C) to glass D4 (712°C). The comparison of the evolution of T_g versus the SiO_2/B_2O_3 ratio for the Ax and Dx series is presented in Fig. 8b. It clearly appears that, whereas the addition of La_2O_3 to Ax glasses without SiO_2 (A0) or with only a small SiO_2 content (A1) induces a decrease of T_g between -11°C (D0) and -3°C (D1), when $SiO_2/B_2O_3 >$ 0.3 the addition of La_2O_3 leads to an increasing difference between the glass transformation temperatures of the two glass series from +3°C between D2 and A3 glasses to +15°C between

D4 and A6 glasses. For transparent glasses of the Bx series (B2-B4) whose B_2O_3 content decreases from 40 to 30 mol% whereas their SiO_2/La_2O_3 ratio remains constant (= 1.2), it appears that T_g increases from 687 to 710°C.

4.3. Crystallization and thermal stability

Except several studies performed on the crystallization of B_2O_3-La_2O_3 binary glasses and more especially on the stoichiometric La-metaborate ($75B_2O_3$-$25La_2O_3$) composition [9,10,70,71,72,73], very few papers deal with the crystallization of B_2O_3-SiO_2-La_2O_3 ternary glasses with a focus only close to the stillwellite ($25B_2O_3$-$25SiO_2$-$25La_2O_3$) composition [11,58]. In recent papers [9,10], we focused on the structure and the mechanism of crystallization of La- and Nd-metaborate glasses by confirming their heterogeneous crystallization tendency and determining the corresponding activation energy with DTA experiments. For binary glasses with La_2O_3 content higher than 25 mol%, the crystallization of La-orthoborate was also observed (in association with LaB_3O_6 as expected from the B_2O_3-La_2O_3 phase diagram [74]), firstly as $LaBO_3$-HT (metastable) that then transforms into $LaBO_3$-LT (stable) with increasing temperature [75]. In their work on the crystallization of glasses with composition close to that of stillwellite (20-35 mol% B_2O_3, 45-60 mol% SiO_2, 20-35 mol% La_2O_3), Sigaev et al. [11,58] indicated that $LaBSiO_5$, $LaBO_3$ and $La_2Si_2O_7$ may crystallize during heating and that $LaBSiO_5$ (stoichiometric stillwellite) preferentially crystallized from glass surface. These authors also specified that because of the high phase separation tendency of the glass compositions they studied, the crystallization of stillwellite was very difficult to control to prepare glass-ceramics in comparison with glasses of similar compositions belonging to the B_2O_3-GeO_2-La_2O_3 ternary system [58].

In the present work, we only focused on the study of the crystallization of the glasses of the Ax series from A0 to A6 during heating by performing DTA experiments on powders (80 - 125

μm) and isochronal heat treatments close to the temperature T_p of the first exothermic DTA peak on powders and quenched plates followed by XRD and Raman spectroscopy characterizations to determine the nature of the crystalline phases formed. In Fig. 9a is shown the evolution of the first exothermic DTA effect for glasses Ax (several weak exothermic effects were also detected at T > 1000°C for the SiO_2-rich glasses but their origin will be not discussed in this paper). A significant shift of T_p towards high temperature is observed as soon as SiO_2 is added to the La-metaborate composition (+47°C between glasses A0 and A1), whereas for higher SiO_2 content (≥ 13.5 mol%) T_p tends to stabilize more or less between 812 and 827°C. Similarly, the DTA peak width firstly increases between glasses A0 and A2 and then tends to stabilize for higher SiO_2 content which indicates that the B_2O_3/SiO_2 substitution induces a decrease of the crystallization rate at least between glasses A0 and A2. As glass stability against devitrification on heating is frequently characterized by the difference $T_x - T_g$ (where T_x is the extrapolated onset crystallization temperature on heating for the first exotherm detected by DTA), the evolution of this difference has been plotted in Fig. 9b for all glasses of the Ax series. It clearly appears that glass stability firstly increases when SiO_2 is substituted for B_2O_3 in the La metaborate glass composition (until 13.5 mol% SiO_2, glass A2) and then decreases.

In order to determine the nature of the phases formed during the first exothermic event, heat treatments have been performed on glasses Ax during 10 min at a temperature close to T_p (heating rate 10°C/min) and then quenched to room temperature. The evolution of the XRD patterns of heat treated glass Ax powders is shown in Fig. 10. Whereas LaB_3O_6 is the only phase that crystallizes in glass A0, the formation of $LaBO_3$-LT is detected as soon as SiO_2 is introduced in the system and this new phase coexists with LaB_3O_6 until composition A4 (22.5 mol% SiO_2). When the amount of SiO_2 becomes ≥ 27 mol% (glass A5), LaB_3O_6 no longer crystallizes and $LaBO_3$ becomes the only crystalline phase formed ($LaBO_3$-LT in glass A5 and a mixture of $LaBO_3$-LT and $LaBO_3$-HT in glass A6). The evolution of Raman spectra of the

heat treated glasses Ax (Fig. 11) shows a crystallization sequence very similar to that put in evidence by XRD. Thus the crystallization phenomena associated with the first exothermic effect along the Ax series can be summarized by the following sequence when increasing SiO_2 content in the glass:

$$LaB_3O_6 \rightarrow LaB_3O_6 + LaBO_3\text{-LT} \rightarrow LaBO_3\text{-LT} \rightarrow LaBO_3\text{-LT} + LaBO_3\text{-HT}$$

It is important to underline that for all glasses Ax, the first exothermic effect observed on the DTA curves after the glass transition temperature T_g on heating is always due to the crystallization of lanthanum borate phases. The crystallization of silicate or borosilicate phases, if it happens, occurs at higher temperatures. Moreover, it is important to indicate that SEM preliminary observations (not shown here) showed that phase separation phenomena (not detected by XRD and Raman spectroscopy) may also occur during heating. This is the case for instance for glass A6 that contains the highest SiO_2 content and for which the separation of SiO_2-rich droplets was observed at the beginning of the exothermic event (799°C).

To complete these results concerning the crystallization tendency of glasses Ax during heating, several results concerning the phases that may crystallize during melt cooling have been obtained. For this, the white zones present on the surface of pieces of glass located outside the space between the metallic plates during melt quenching (i.e. pieces of glasses that were not efficiently quenched) were analyzed by Raman spectroscopy. It clearly appeared (spectra not shown) that whereas LaB_3O_6 was the only crystalline phase detected in the white zones for glass A0, for all glasses containing SiO_2 (A1-A6) no LaB_3O_6 crystallization was observed and $LaBO_3$-LT was always the main crystalline phase formed.

5. Discussion

5.1. Extension of the glass domain

A relatively large composition domain where homogeneous transparent glasses can be obtained has been put in evidence in this work within the SiO_2-B_2O_3-La_2O_3 ternary system using a melt quenching with a rate close to 10^4°C/min (Fig. 3). This glass domain, significantly wider than those already prospected by Sigaev et al. [11] (close to the stillwellite $LaBSiO_5$ composition) and Levitskii et al. [12] (Fig. 1), is limited by glass-in-glass immiscibility for the highest SiO_2 and/or B_2O_3 concentrations and by high crystallization tendency of lanthanum borate and borosilicate phases for the highest La_2O_3 concentrations during melt quenching. The separation tendency of a La_2O_3-poor glassy phase observed at the SiO_2 and/or B_2O_3-rich boundary, leading to opalescent or totally opaque samples, is probably related to the existence of an immiscibility gap all along the join SiO_2-B_2O_3 in the ternary diagram due to the tendency towards phase separation of the corresponding SiO_2-La_2O_3 and B_2O_3-La_2O_3 binary systems (the extension of the phase separation field for these two systems is shown by the two lines outside the diagram in Fig. 3) [25,26]. Upon increasing the amount of La_2O_3, the impossibility to obtain glasses can be explained both by the rapid and strong increase of the liquidus temperature (by analogy with what occurs in the SiO_2-La_2O_3 and B_2O_3-La_2O_3 systems when La_2O_3 content is higher than about 30 mol%) [25,26] and by the increasing amount of highly depolymerized (i.e. bearing a high proportion of NBOs) and mobile units present in the melt, such as orthoborate (isolated $(BO_3)^{3-}$) and pyroborate (dimer $(B_2O_5)^{4-}$) units that have been put in evidence by Raman spectroscopy in our La_2O_3-rich quenched ternary glasses [75] and in La_2O_3-rich binary B_2O_3-La_2O_3 glasses by Kajinami et al. [76] (La_2O_3 is a modifier oxide leading to NBOs formation in the borosilicate network by acid-base reaction with network formers, it is the only modifier oxide in our glasses). The high crystallization tendency in La_2O_3-rich samples (C6, F0, F1, F2, B5) of $LaBO_3$, $La_3Si_2BO_{10}$ and/or $La_2Si_2O_7$ phases whose structures are made of highly depolymerized units ($(BSiO_6)^{5-}$ (with 5NBOs + 1BO), $(BO_3)^{3-}$ (with 3NBOs) and $(Si_2O_7)^{2-}$ (with 6NBOs) groups respectively) as presented in Section 2.1 (Table 1, Fig. 2b), is in

agreement with this last hypothesis. Moreover, the proximity of $LaBO_3$ and $La_3Si_2BO_{10}$ compositions to the La_2O_3-rich limit of the glass domain (Figs. 1 and 3) suggests that these phases are probably the first phases that crystallize during melt cooling in the ternary system as it is the case for $LaBO_3$ in the B_2O_3-La_2O_3 system for compositions with La_2O_3 content ranging from 28 to 50 mol% [25].

It is important to underline that the composition range of transparent glasses in the ternary system put in evidence in the present work starts from the glassy domain of B_2O_3-La_2O_3 binary system (between 22 and 33 mol% La_2O_3, C10-C7) around the lanthanum metaborate composition which is known to easily vitrify [7,10] and then by adding SiO_2 (C1, C2, C12, C13) or substituting B_2O_3 with SiO_2 (A1-A6, D1-D4) to these B_2O_3-La_2O_3 binary glasses, it is possible to extend this binary glass domain in the ternary system and to obtain transparent glasses bearing increasing SiO_2 content (but no more than 40 mol%). Different reasons may explain the impossibility to obtain clear glasses and even to vitrify the melt for higher SiO_2 content and thus to extend the ternary glass domain. The very high liquidus temperatures in the binary SiO_2-La_2O_3 phase diagram [26] ($T_{liquidus} \geq 1625°C$) suggests that $T_{liquidus}$ probably significantly increases for SiO_2-rich ternary compositions making it more and more difficult to obtain glasses when increasing SiO_2 concentration. Moreover, the increasing depolymerization of the network (i.e. the increase of the NBOs proportion, due to the decrease of BO_4 units induced by increasing the SiO_2 proportion as shown by ^{11}B MAS NMR (Fig. 12a,c) and discussed in the next section) may also explain the difficulty to maintain long-range disorder during melt quenching. Fig. 3 also shows that it is also possible to synthesize clear glasses, by varying the amount of B_2O_3 and keeping constant the SiO_2/La_2O_3 ratio (samples B1-B4 and S1-D4-S2). Although some compositions, close to stillwellite (E5), were reported as glassy and transparent in literature [11], it was not possible to obtain clear glasses in this region of the diagram in the present work despite several attempts as already explained in the experimental

section. Indeed, the samples near the stillwellite composition (E1-E5) all exhibit partial or total glass-in-glass phase separation (Fig. 4c,d and 5a,b). For instance, the stoichiometric stillwellite composition leads to a phase separated microstructure which could indicate a spinodal decomposition (Fig. 5a). The reason for the difference between our results and the ones of Sigaev et al. [11] remain unclear but could be explained by the fact that these authors mainly used corundum crucibles to melt their samples which could lead to melt pollution by Al_2O_3 and would make easier to obtain clear glasses during quenching (inhibition of phase-separation).

5.2. Evolution of glass transformation temperature

A significant evolution of T_g with glass composition has been put in evidence for the different glass series Ax, Bx and Dx (Fig. 8). This evolution is linked to changes in glass structure and chemical bonding when the SiO_2/B_2O_3 ratio or the La_2O_3 content increases. For instance, from the ^{11}B MAS NMR study of glasses of Ax, Bx and Dx series, the evolution with composition of the relative proportions of BO_3, BO_4 and SiO_4 units shown in Fig. 12 has been obtained. As example the ^{11}B MAS NMR spectra of glasses of the Dx series are shown in Fig. 13a with an example of simulation in Fig. 13b (glass D2) used to extract the relative proportions of BO_3 and BO_4 units according to the method described in a previous paper [10]. The ^{11}B NMR parameters (isotropic chemical shift δ_{iso}, quadrupolar coupling constant C_q and quadrupolar asymmetry parameter η_q) deduced from the simulation of the spectrum of glass D2 are given in the legend of Fig. 13. ^{11}B NMR parameters of glass A0 (La metaborate) were given in [10]. For all other ternary and binary glasses prepared in this study, ^{11}B NMR parameters (not useful in the discussion of the present work) will be presented in another paper.

For the Ax series (Fig. 12a), the B_2O_3/SiO_2 substitution induces a continuous decrease of the proportion of BO_4 units whereas the proportion of BO_3 units (that may bear NBOs) slightly decreases only above 22.5 mol% SiO_2 (A4) and the proportion of SiO_4 units progressively

increases along the series. As BO_4 units act as reticulating groups in borate and borosilicate networks (assuming that BO_4 units do not bear NBOs [77]), the decrease of their concentration induces a depolymerization of the borosilicate network (increase of NBOs content), since the proportion of modifier oxide (La_2O_3) does not decrease along the Ax series (on the contrary the La_2O_3 content slightly increases, Table 2). Indeed, the continuous decrease of the proportion of BO_4 units indicates that along the series La_2O_3 interacts more with the borosilicate network by transferring oxygen anions to BO_3 or SiO_4 units to form NBOs. Thus, the structural role of La^{3+} ions progressively changes, these ions acting more and more in as modifiers located close to NBOs associated with SiO_4 or BO_3 units, and less and less as charge compensators near BO_4 units. This depolymerization is expected to induce a decrease of T_g. On the contrary, the increase of the proportion of SiO_4 units along the Ax series, together with the decrease of the proportion of BO_3 units observed above 22.5 mol% SiO_2, are expected to lead to an increase of T_g, because tetrahedral SiO_4 units increase glass dimensionality when they replace triangular BO_3 units. Indeed, it is known that for oxide glasses T_g increases with the cross-link density of the network, with the strength of the bond and with the tightness of the packing in the network [78]. To explain the evolution shown in Fig. 8 for the Ax series, we propose that the decrease of T_g, expected because of the depolymerization induced by the decrease of BO_4 units, is compensated or dominated by two effects:

- The replacement of BO_3 units by SiO_4 units, that strengthens the network by increasing its dimensionality,
- The La^{3+} ions in modifying positions are more tightly bound to the borosilicate network, than La^{3+} ions in charge-compensating positions close to BO_4 units because of the higher local negative charge carried by NBOs. Then, the strengthened La^{3+}- O bonds may also contribute to the increase of T_g.

Only the second effect (La^{3+}- O bond strengthening) would be effective in the first part of the Ax series (A0 to A3), while both effects add together in the last part of the Ax series (A4 to A6), explaining the plateau followed by the T_g increase in Fig. 8 when the SiO_2/B_2O_3 ratio increases. The slight increase of La_2O_3 content along the Ax series (+ 4.7 mol%, Table 2) may also partly contribute to the increase of T_g.

As for the Dx series, the amount of La_2O_3 is higher than for the Ax series. The continuous increase of T_g when the SiO_2/B_2O_3 ratio increases (+46°C) suggests that the strengthening effect due to La^{3+} ions dominates all along the Dx series (Fig. 8b). Indeed, according to Fig. 12c, it appears that the amount of BO_4 units decreases with the SiO_2 content but remains significantly smaller for the Dx series than for the Ax series (Fig. 12a).

For the Bx series, when the B_2O_3 content decreases, the proportion of SiO_4 units increases at the expense of BO_4 units and the proportion of BO_3 units remains almost constant (Fig. 12b). As the amount of La_2O_3 remains high for all transparent Bx glasses (26.3- 31.2 mol%), it is expected that the La^{3+}- O bond strengthening effect due to this structural evolution (location of more and more La^{3+} ions in a modifying position close to NBOs instead of in a charge-compensating position close to BO_4 units) would be at the origin of the increase of T_g when the B_2O_3 content decreases (Fig. 8a).

It can be underlined that the T_g values of all La borosilicate glasses always remain significantly higher than those of alkali borosilicate glasses for which T_g always remains lower than 600°C [79,80]. This difference can be explained by the high field strength of RE^{3+} ions in comparison with alkali ions which are less strongly bonded to NBOs.

5.3. Crystallization and thermal stability

An important evolution of the nature of the phases crystallizing first during heating glasses of the Ax series has been put in evidence (Figs. 10 and 11), with LaB_3O_6 - the unique phase that

crystallizes in glass A0 - becoming less and less abundant in favor of $LaBO_3$ when SiO_2 content increases. This progressive modification of the type of La-borate crystallizing in the undercooled melt - less than 140°C above T_g (Fig. 9b) - can be explained by structural considerations on glasses by comparison with the borate units that compose the structure of LaB_3O_6 and $LaBO_3$ crystals. The evolution of the relative proportions of BO_4, BO_3 and SiO_4 units determined by ^{11}B MAS NMR and shown in Fig. 12a indicates that along the Ax series the proportion of BO_4 units is reduced by 55% between compositions A0 and A6 whereas the proportion of BO_3 units only decreased by about 20%. As the structure of LaB_3O_6 crystals consists of chains composed of BO_4 and BO_3 units in a 1:2 ratio [39], the progressive decrease of the availability of BO_4 units in the undercooled melt can explain the increasing difficulty of their crystallization when the SiO_2 content increases. Furthermore, the fact that BO_3 units always remain the main structural units present in glasses Ax (always higher than 47%, Fig. 12a) and that these units are more and more associated with NBOs along the series, according to the discussion presented in section 5.2, may explain the preferential crystallization of $LaBO_3$ for the SiO_2-rich glasses Ax. Indeed, this crystalline phase is only constituted of highly depolymerized $(BO_3)^{3-}$ orthoborate entities (total absence of BO_4 entities in the structure) [31]. The evolution of glass stability presented in Fig. 9b, that exhibits a maximum around 14 mol% SiO_2, may be explained as follow. The fact that glass A0 has the same composition LaB_3O_6 as the phase that crystallizes (congruent crystallization) may explain that it is the less stable (Fig. 9b) and the one that crystallizes the fastest of the series (its DTA signal is the most intense of the series, Fig. 9a). The progressive B_2O_3/SiO_2 substitution, that brings chemical and structural complexity (increasing proportion of SiO_4 units and formation of B-O-Si connections) and that induces a continuous decrease of the amount of BO_4 units available in the undercooled melt (Fig. 12a), will hinder the nucleation and growth of La-metaborate crystals and will thus increase glass stability which would explain the increasing part of the curve (Fig. 9b). When

SiO_2 content increases, the glass structure becomes more and more depolymerized (see section 5.2), with probably the presence of mobile $(BO_3)^{3-}$ units as in binary B_2O_3-La_2O_3 glasses [10,76]. This may explain the increasing crystallization tendency of $LaBO_3$ and thus the origin of the decreasing part of the glass stability curve. Nevertheless, due to the increasing chemical and structural complexity that limits the growth rate of $LaBO_3$ crystals in the presence of an increasing amount of SiO_4 units, the DTA signal associated with $LaBO_3$ crystallization appears broad and weakly intense (Fig. 9a).

By comparing glass stability with crystallization tendency during melt cooling for glasses Ax, it appeared that, whereas LaB_3O_6 and then $LaBO_3$ were the first phases crystallizing during glass heating along the series, during melt cooling the crystallization of LaB_3O_6 was only put in evidence for glass A0 while only $LaBO_3$ crystals were detected for glasses A1-A6. The lack of LaB_3O_6 crystallization during melt cooling of SiO_2-bearing glasses may be explained by the decrease of the amount of BO_4 units in the melt due to both the B_2O_3/SiO_2 substitution as put in evidence by ^{11}B MAS NMR study of glasses (Fig. 12a) and the fact that in borate and borosilicate melts the BO_4/BO_3 ratio decreases with temperature [81]. As a consequence, the increase of melt depolymerization and probably the increasing amount of mobile $(BO_3)^{3-}$ units would explain the preferential crystallization of $LaBO_3$ during melt cooling at the expense of LaB_3O_6. This preferential crystallization is also in agreement with the fact that $LaBO_3$ is more refractory than LaB_3O_6 (melting temperature: $LaBO_3$ (1660°C), LaB_3O_6 (1141°C) [25]) and is thus expected to form before La metaborate during melt cooling.

Finally, it is interesting to remark that when the composition of glasses Ax approaches that of stillwellite (E5, Fig. 3), the BO_4/BO_3 proportions ratio determined by ^{11}B MAS NMR becomes low (for instance for glass A6 this ratio reaches 0.39, Fig. 12a). This low proportion of BO_4 units may be at the origin of the difficulties encountered by Sigaev et al. [58] to prepare stillwellite glass-ceramics from glasses with composition close to stillwellite and may explain

the preferential heterogeneous nucleation that occurs in theses glasses. Indeed, as stillwellite crystal is only composed of BO_4 units (see Section 2.1), the structure of these glasses and that of the crystalline phase of close composition are strongly different which may explain the lack of bulk nucleation and the difficulties encountered to prepare stillwellite glass-ceramics in addition to the difficulties we put in evidence to obtain homogeneous glasses from such melts composition.

6. Conclusion

For the first time, the glass formation domain in the ternary diagram SiO_2-B_2O_3-La_2O_3 was extensively studied using a melt quenching method (quenching rate ~ 10^4°C/min). The extension of the vitrification domain is clearly related to the tendency towards phase separation and crystallization within the corresponding SiO_2-La_2O_3 and B_2O_3-La_2O_3 binary diagrams. The evolution of the glass transformation temperature among this domain has been studied and correlated with changes that occur in glass structure: the increasing amount of depolymerized borate and silicate entities associated with a strong decrease of the proportion of BO_4 entities (as shown by ^{11}B NMR) and the consecutive evolution of the structural role of La^{3+} ions when silica content increases. The study of glass stability during heating revealed that, for a glass series with increasing SiO_2/B_2O_3 ratio extending along the glass domain, it is always La-borate phases (firstly mainly LaB_3O_6 and then $LaBO_3$) that crystallize first, even for the compositions richest in silica. This effect could be explained by the important decrease of the amount of BO_4 units (present in the structure of LaB_3O_6 crystals) and the increasing proportion of depolymerized BO_3 units (such as $(BO_3)^{3-}$ that are the only borate entities present in the structure of $LaBO_3$ crystals) when the SiO_2 content increases.

Because of their relativity large domain of composition (0 - 38 mol% SiO_2), their high transformation temperature range (T_g > 660°C), their good thermal stability, their low

hygroscopicity and probably their good chemical durability against water alteration due to their high rare earth oxide concentration and finally the possibility to partly substitute La by optically active RE in their structure, such La_2O_3-B_2O_3-SiO_2 ternary glasses could find applications in various fields such as optics. Moreover, as RE_2O_3, SiO_2 and B_2O_3 are abundant oxides present in the composition of borosilicate nuclear glasses, La_2O_3-B_2O_3-SiO_2 ternary glasses can be considered as very simplified models of such glasses (without alkali and alkaline-earth oxides) to better understand the impact of La_2O_3 addition (as fission product and only modifier oxide) on the structure of the borosilicate network.

Acknowledgments

The authors gratefully acknowledge the Réseau Francilien sur les oxydes fonctionnels (DIM OxyMORE) and the Région Ile de France for the PhD grant of H. Trégouët. The Areva Chaire with Chimie-ParisTech and ENSTA-ParisTech is gratefully acknowledged for its financial support. The authors also gratefully acknowledge M. Fialin (CAMPARIS service, Paris, France) for his help during EPMA measurements. The authors would particularly like to thank P. Lehuédé (C2RMF, Paris, France) for his availability and precious help during SEM observations.

Formula	**$RESiBO_5$**	**$RE_3Si_2BO_{10}$**	**$RE_{10}Si_4B_2O_{26}$**
Mineralogical name	Stillwellite	-	Oxyapatite
RE	La, Ce, Pr, Nd, Sm	La, Ce, Nd, Sm, Eu, Gd, Dy	Y, La, Pr, Nd, Sm, Eu, Gd, Dy, Tb
Space group	$P3_1$	Pbca	$P6_3/m$
B coordination	4	3	4
NBO/B atom	0	2	4
B-O distances (Å)	1.37-1.58 (1.48) [38]	1.329-1.475 (1.384) [51]	1.557-1.615 (1.593)[a] [53]
Q^n units (SiO_4)	Q^2	Q^0, Q^1	Q^0
Si-O distances (Å)	1.586-1.659 (1.623) [38]	1.627-1.650 (1.638) [51]	1.557-1.615 (1.593)[a] [53]
La coordination	9 [38] [b]	8 (La1) - 9 (La2 et 3)	7 (6h) - 9 (4f)
La-O distances	2.412-2.762 (2.591) [38]	2.395-2.697 (2.588) [51]	2.304-2.825 (2.515-2.605) [53]
Anionic groups	Helical chains of BO_4 linked to $[SiO_4]^{2-}$	$[BSiO_6]^{5-}$, $[SiO_4]^{4-}$	$[SiO_4]^{4-}$, $[BO_4]^{5-}$, O^{2-}
References	[36,38,40,41,82,83]	[47,48,49,50,51]	[53,54,55,56]

Table 1. Overview of the crystalline phases containing both Si, B and RE reported in the ternary system SiO_2-B_2O_3-RE_2O_3 from literature. Average distances are given in parenthesis. ([a]) Si and B share the same site in oxyapatite and thus the distances given here correspond to the average site. ([b]) According to Chi et al. [38] and Burns et al. [37] RE is located in 9-coordinated sites in the stillwellite structure whereas according to Ono et al. [40] RE would be located in 10-coordinated sites in the same structure. Voronko et al. [36] also reported that Ce is 9-fold coordinated in Ce-stillwellite ($CeBSiO_5$). This discrepancy between authors concerning RE

coordination may be explained by the fact that contrarily to the other authors [37,38], Ono et al. [40] did not envisage the fact that one O site in the surrounding of RE could be split in two sites with partial occupancies.

Sample	Composition			T_g (°C)	Remarks
	SiO_2	B_2O_3	La_2O_3		
A0	0	75 (74.1)	25 (25.9)	677	CG
A1	9 (8.9)	65 (63.2)	26 (27.8)	677	CG
A2	13.5	60	26.5	674	CG
A3	18 (17.9)	55 (54.3)	27 (27.8)	678	CG
A4	22.5	50	27.5	681	CG
A5	27 (27.2)	45 (43.3)	28 (29.5)	686	CG
A6	36 (35.5)	35 (33.9)	29 (30.6)	697	CG
B0	30	45	25	686	PS
B1	31.2	42.5	26.3	n.m.	CG
B2	32.5	40	27.5	687	CG
B3 (=A6)	36 (35.5)	35 (33.9)	29 (30.6)	697	CG
B4	38.8	30	31.2	710	CG
B5	46.5	25	33.5	-	CG + X (α, β, γ)
D0	0	67 (64.5)	33 (35.5)	666	CG + X (β)
D1	8.3 (8.3)	59 (56.3)	32.7 (35.4)	674	CG + X (β)
D2	16.4 (16.3)	50 (48.6)	33.6 (35.1)	681	CG + X (β)
D3	24.5 (24.4)	41 (39.7)	34.5 (35.9)	695	CG + X (α, β)
D4	33.5	32.5	34	712	CG

Table 2. Nominal compositions (in mol%) of the samples of the Ax, Bx and Dx series along with T_g for the glassy samples. For several samples, the true composition (in mol%) was determined by EPMA (values given in parenthesis). Remarks concerning clearness and crystallization of the samples (according to characterization by XRD and Raman spectroscopy) are indicated in the last column (CG: Clear Glass, PS: Phase Separation, X: Crystallization (α: $La_3Si_2BO_{10}$, β: $LaBO_3$-HT or/and $LaBO_3$-LT, γ: $La_2Si_2O_7$). - : not measured. The error in the determination of T_g (onset point on the DTA curves) is estimated close to ± 2°C. Uncertainties on EPMA determinations: SiO_2 (0.2 - 0.5 mol%), B_2O_3 (1 - 2 mol%), La_2O_3 (0.1 - 0.2 mol%).

Sample	Composition			T_g (°C)	Remarks
	SiO_2	B_2O_3	La_2O_3		
C0 (=A0)	0	75 (74.1)	25 (25.9)	677	CG
C1	4.8	71.4	23.8	673	CG + X (β)
C2	9.1	68.2	22.7	671	CG
C3	13.1	65.2	21.7	-	PS
C4	19.4	59.1	21.5	-	PS
C5	24.3	54.1	21.6	-	PS
C6	0	65	35	-	X (β)
C7	0	67 (64.5)	33 (35.5)	666	CG + X (β)
C8	0	70 (68.2)	30 (31.8)	667	CG + X (β)
C9	0	72	28	666	CG + X (β)
C10	0	78 (76.5)	22 (23.5)	674	CG
C11	0	82 (78.4)	18 (21.6)	679	PS
C12	4.8	66.7	28.5	-	CG + X (β)
C13	4.7	74.3	21	-	CG
C14	4.8	78.1	17.1	-	PS
S1	30.9	37.8	31.3	697	CG + X (β)
S2	35.9	27.8	36.3	-	CG + X (α, β)
E0	38.5	37.5	24	-	PS
E1	41	32.5	26,5	-	PS
E2	45	27.5	27.5	710	PPS
E3	43.3	35	21.7	-	PS
E4	46.7	30	23.3	-	PPS + CG
E5	50 (51.3)	25 (23)	25 (25.7)	716	PS
F0	7.6	53.6	38.8	-	X (β)
F1	22.3	37.2	40.5	-	X (α, β)
F2	30.9 (31.3)	30.1 (28)	39 (40.7)	-	X (α, β)
G0	80	20	-	-	CG
G1	79.19	19.8	0.01	-	PS

Table 3. Nominal compositions (in mol%) of the samples of the Cx, Dx, Ex, Fx and Gx series along with T_g for the glassy samples. For several samples, the true composition (in mol%) was determined by EPMA (values given in parenthesis). Remarks concerning clearness and crystallization of the samples (according to characterization by XRD and Raman spectroscopy)

are indicated in the last column (CG: Clear Glass, PS: Phase Separation, PPS: Partial Phase Separation X: Crystallization (α: $La_3Si_2BO_{10,}$ β: $LaBO_3$-HT or/and $LaBO_3$-LT). - : not measured. The error in the determination of T_g (onset point on the DTA curves) is estimated close to ± 2°C. Uncertainties on EPMA determinations: SiO_2 (0.2 - 0.5 mol%), B_2O_3 (1 - 2 mol%), La_2O_3 (0.1 - 0.2 mol%).

Figures caption

Figure 1. Ternary SiO_2-B_2O_3-La_2O_3 diagram showing the compositions (in mol%) studied in literature [11,12] to prepare glasses. The glasses reported in the binary B_2O_3-La_2O_3 system by Chakraborty et al. [7] are also indicated (melts were cooled in air in the crucibles). The nature of the samples reported is referred as glassy (transparent, phase-separated) or containing crystals using different symbols. Green circles and squares correspond respectively to the transparent glasses reported by Levitskii et al. [12] (without indication about the quenching method and rate) and Sigaev et al. [11] (rapid quenching of melt between metallic plates). The binary and ternary glassy domains are surrounded by dotted lines. The crystalline phases reported in literature (see Section 2.1) for both binary and ternary systems are also indicated: LaB_3O_6 (a), $LaBO_3$ (b), La_3BO_6 (c), La_2SiO_7 (d), $La_{9.33}Si_6O_{26}$ (e), La_2SiO_5 (f), $La_{9.66}Si_5BO_{26}$ (g), $La_{10}Si_4B_2O_{26}$ (h), $La_3Si_2BO_{10}$ (i), $LaBSiO_5$ (j).

Figure 2. Crystalline structure of: (a) $LaBSiO_5$ showing the helical chains of BO_4 and SiO_4 units along the 3_1 axis, (b) $La_3Si_2BO_{10}$ showing the isolated $[SiO_4]^{4-}$ tetrahedra and $[BSiO_6]^{5-}$ entities (associating a $[SiO_4]^{4-}$ tetrahedron and a BO_3 triangle), (c) $La_{10}Si_4BO_{26}$ showing the isolated BO_4 and SiO_4 tetrahedral units (both in green in the figure). The isolated O^{2-} ions existing in the structure have not been shown in Fig. 2c. The direction of (a,b,c) crystallographic axis are given for each representation. These figures were drawn from the structural data given in references [38,51,53].

Figure 3. Ternary SiO_2-B_2O_3-La_2O_3 diagram showing the compositions melted and quenched in the present work. The nature of the samples obtained in this work (after macroscopic and microscopic observations and XRD characterization) is referred to as glassy (transparent,

partially or totally phase separated) or containing crystals using different symbols. The glassy domain (transparent glasses) put in evidence in this work is surrounded by dotted lines. The different colors (red, blue, and green) correspond to the different glass series (Ax, Dx, Bx respectively). The fields of phase separation of binary B_2O_3-La_2O_3 and SiO_2-La_2O_3 systems [25,26] are also indicated (blue bold lines outside the diagram).

Figure 4. Macroscopic aspect of several samples of the SiO_2-B_2O_3-La_2O_3 ternary system obtained after melting and quenching: (a,b) composition $36SiO_2$-$35B_2O_3$-$29La_2O_3$ (A6=B3), exhibiting complete transparency; (c) composition $45SiO_2$-$27.5B_2O_3$-$27.5La_2O_3$ (E2) showing partial phase separation; (d) composition $50SiO_2$-$25B_2O_3$-$25La_2O_3$ (E5) exhibiting total phase separation; (e) composition $24.5SiO_2$-$41B_2O_3$-$34.5La_2O_3$ (D3) clear glass along with partial crystallization of $La_3Si_2BO_{10}$ and $LaBO_3$; composition $22.3SiO_2$-$37.2B_2O_3$-$40.5La_2O_3$ (F1) totally opaque sample with crystallization of $La_3Si_2BO_{10}$ and $LaBO_3$. Pressing between metallic plates (a,c,d,e,f) or natural cooling in the Pt crucible outside the furnace (b).

Figure 5. SEM (BSE) images of several samples of the SiO_2-B_2O_3-La_2O_3 ternary system obtained after melting and quenching: (a) composition $50SiO_2$-$25B_2O_3$-$25La_2O_3$ (E5) exhibiting phase separation (aspect of spinodal decomposition), see Fig. 3d; (b) composition $46.7SiO_2$-$30B_2O_3$-$23.3La_2O_3$ (E4) exhibiting phase separation; (c) composition $31.25SiO_2$-$42.5B_2O_3$-$26.25La_2O_3$ (B1) exhibiting slight phase separation in limited areas of the sample; (d) composition $80SiO_2$-$20B_2O_3$ + 1mol% La_2O_3 (G1) exhibiting phase separation; (e) composition $8.3SiO_2$-$59B_2O_3$-$32.7La_2O_3$ (D1) exhibiting crystallization of $LaBO_3$ in limited areas of the sample; (f) composition $7.6SiO_2$-$53.6B_2O_3$-$38.8La_2O_3$ (F0) exhibiting crystallization of $LaBO_3$ throughout the sample. The dark droplets in (b,c) are La depleted whereas the light ones in (d) are La-rich. $LaBO_3$ crystals appear in white in the SEM images (e,f) because of La-enrichment in comparison with their surroundings.

Figure 6. Examples of XRD patterns of ternary samples (F0,F2,S2) showing the crystallization of $La_3Si_2BO_{10}$ (□), $LaBO_3$-LT (○) and/or $LaBO_3$-HT (■). The XRD patterns of several reference crystalline phases prepared for this study are also shown for comparison: $La_3Si_2BO_{10}$ (JCPDS 01-071-6609), $LaBO_3$-LT (JCPDS 04-013-4216), $LaBO_3$-HT (JCPDS 00-008-0193), $LaBSiO_5$ (JCPDS 00-019-0659), $La_{10}Si_4BO_{26}$ (JCPDS 00-052-0699). The presence of $La_3Si_2BO_{10}$ impurity is detected in $LaBSiO_5$ (*).

Figure 7. Examples of Raman spectra of ternary samples (F0,F2) exhibiting strong crystallization during quenching and of several reference crystalline phases ($LaBO_3$-LT (□) and HT (●), $La_3Si_2BO_{10}$ (♦)) synthesized for this study. The presence of $La_2Si_2O_7$ (○) in F2 was made by comparison with the Raman spectrum shown in reference [84]. The presence of apatite crystals ($La_{10}Si_4BO_{26}$, $La_{9.66}Si_5BO_{26}$) in F2 sample cannot be excluded. (◊: band non-attributed).

Figure 8. (a) Evolution of T_g with nominal B_2O_3 content for glasses of the Ax (●), Dx (Δ) and Bx (○) series. (b) Evolution of T_g with the nominal SiO_2/B_2O_3 concentration ratio for glasses of the Ax and Dx series. The dotted lines shown in (b) are guides for the eye to facilitate the comparison of the evolution of T_g for glasses of the Ax and Dx series.

Figure 9. (a) Evolution of the DTA curves (between 600 and 1000°C) of glasses Ax showing the evolution of the first exothermic effect with glass composition (particle size: 80 - 125 µm; heating rate: 10°C/min). The amplitude of the variation of T_g of glasses Ax (674 - 697°C, Table 2) is also shown in the figure. (b) Evolution of (T_x - T_g) with the SiO_2 nominal content of glasses Ax. T_x is the extrapolated onset crystallization temperature on heating for the first exotherm detected by DTA

Figure 10. XRD patterns of glasses of the Ax series after heat treatment of powders (80-125µm) during 10 min at a temperature close to T_p (first exothermic effect on the corresponding DTA

curves, Fig. 20) : 766°C (A0), 812°C (A1), 828°C (A2), 826°C (A3), 827°C (A4), 812°C (A5) and 816°C (A6). The crystallization of LaB_3O_6 (♦) (JCPDS 00-023-1140) in A0-A4, $LaBO_3$-LT (●) (JCPDS 04-013-4216) in A1-A6 and $LaBO_3$-HT (○) (JCPDS 00-008-0193) in A6 is put in evidence (see Fig. 6 for the XRD patterns of $LaBO_3$-BT and -HT).

Figure 11. Raman spectra of glasses of the Ax series (quenched plates) after heat treatment during 10 min at a temperature close to T_p (first exothermic effect on the corresponding DTA curves, Fig. 20): 766°C (A0), 812°C (A1), 828°C (A2), 826°C (A3), 827°C (A4), 812°C (A5) and 816°C (A6). The crystallization of LaB_3O_6 (♦) in A0-A3, $LaBO_3$-LT (●) in A1-A6 and $LaBO_3$-HT (○) in A6 is put in evidence. For comparison, the Raman spectra of the corresponding reference crystalline phases (LaB_3O_6, $LaBO_3$-LT, $LaBO_3$-HT) are also given at the bottom of the figure.

Figure 12. Evolution with glass composition (nominal SiO_2 or B_2O_3 contents) of the relative proportion of BO_3, BO_4 and SiO_4 units (BO_3 and BO_4 proportions were deduced from ^{11}B MAS NMR analysis (see Fig. 13b) whereas SiO_4 proportion was calculated from glass composition) for glasses of the Ax (a), Bx (b) and Dx (c) series. For SiO_4 proportion calculations for the different series, the analyzed SiO_2 content was used when available (Table 2).

Figure 13. (a) Evolution of ^{11}B MAS NMR spectra of glasses of the Dx series. (b) Contributions of BO_3 and BO_4 units to the simulated spectrum of glass D2. The following NMR parameters were deduced from this simulation: BO_3 (75.1%, δ_{iso} = 19.46 ppm, C_q = 2.69 MHz, η_q= 0.48), BO_4 (24.9%, δ_{iso} = 1.42 ppm, C_q = 0.5 MHz, η_q = 0.6).

Figure 1

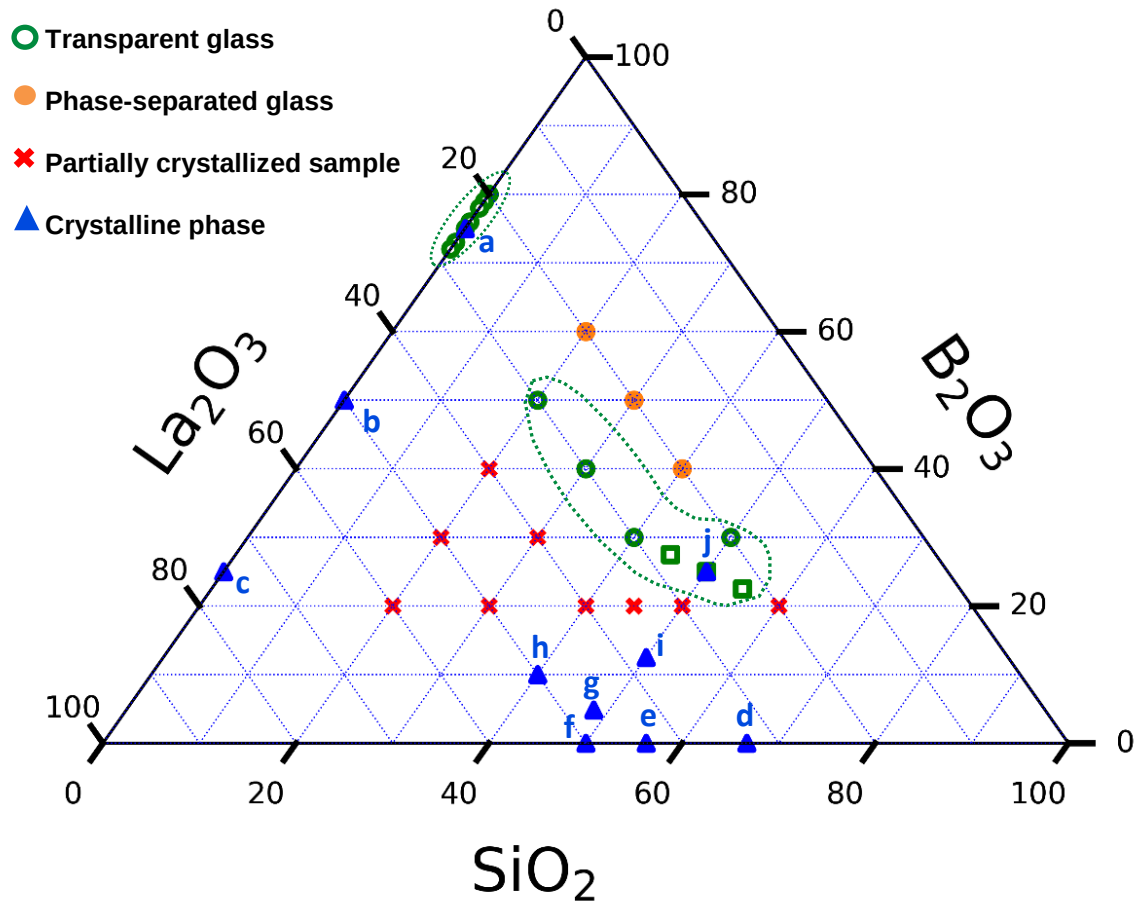
Transparent glass
Phase-separated glass
Partially crystallized sample
Crystalline phase
La2O3
B2O3
SiO2
0
20
40
60
80
100
a
b
c
d
e
f
g
h
i
j

Figure 2

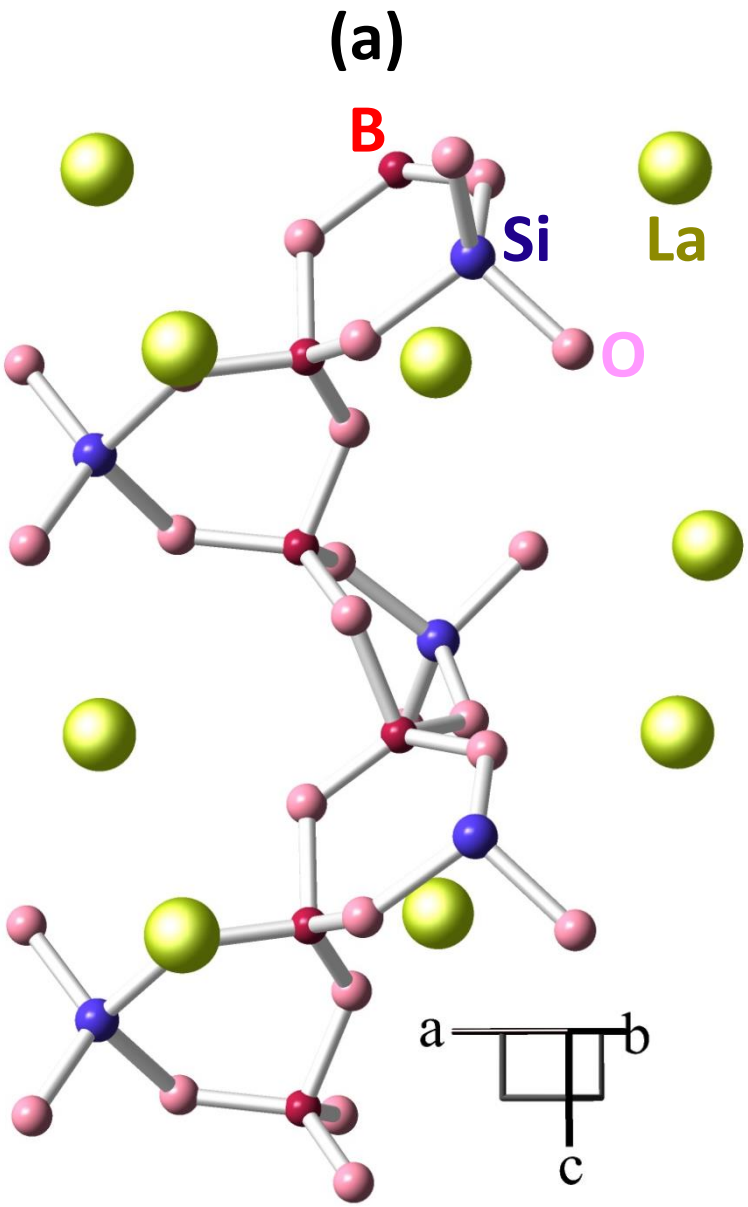

Figure 2 (continue)

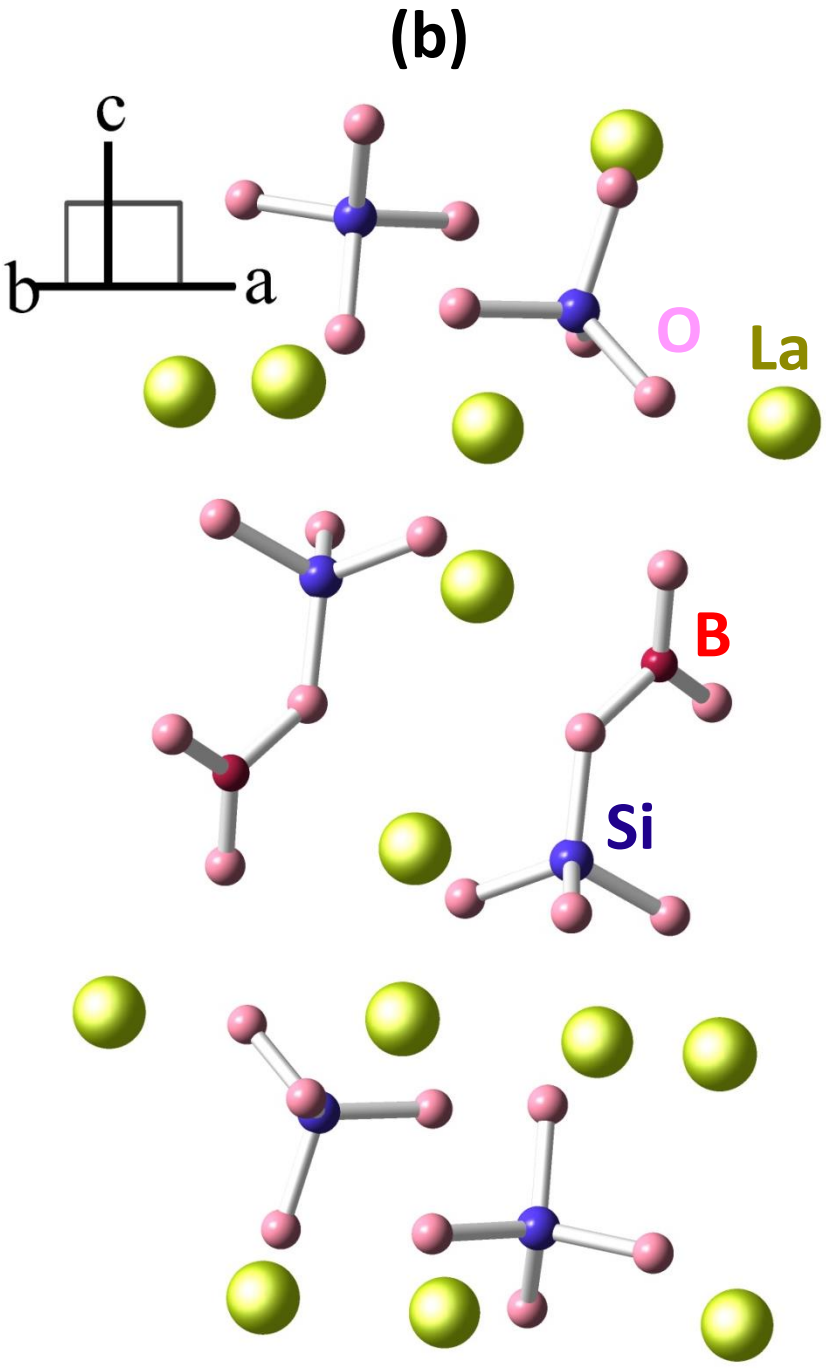

Figure 2 (continue)

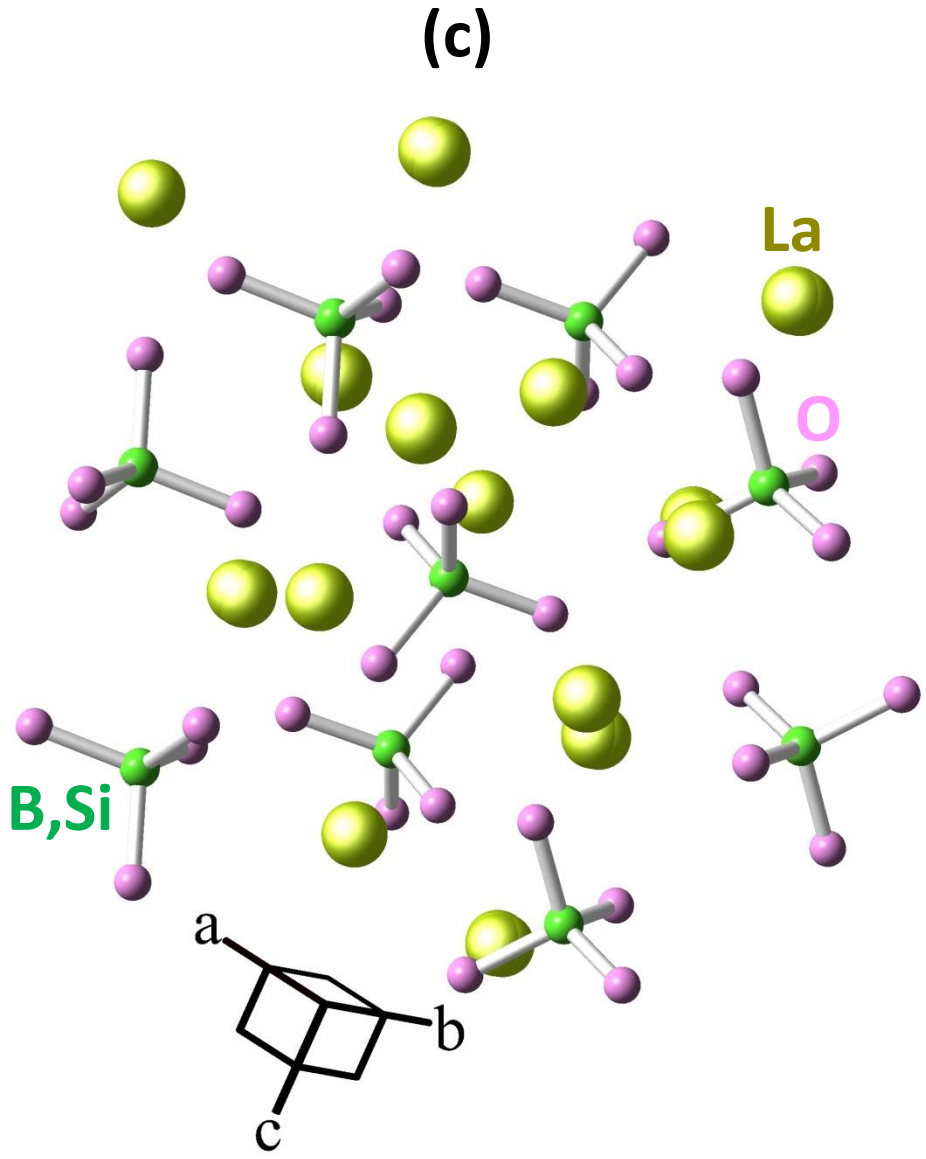

Figure 3

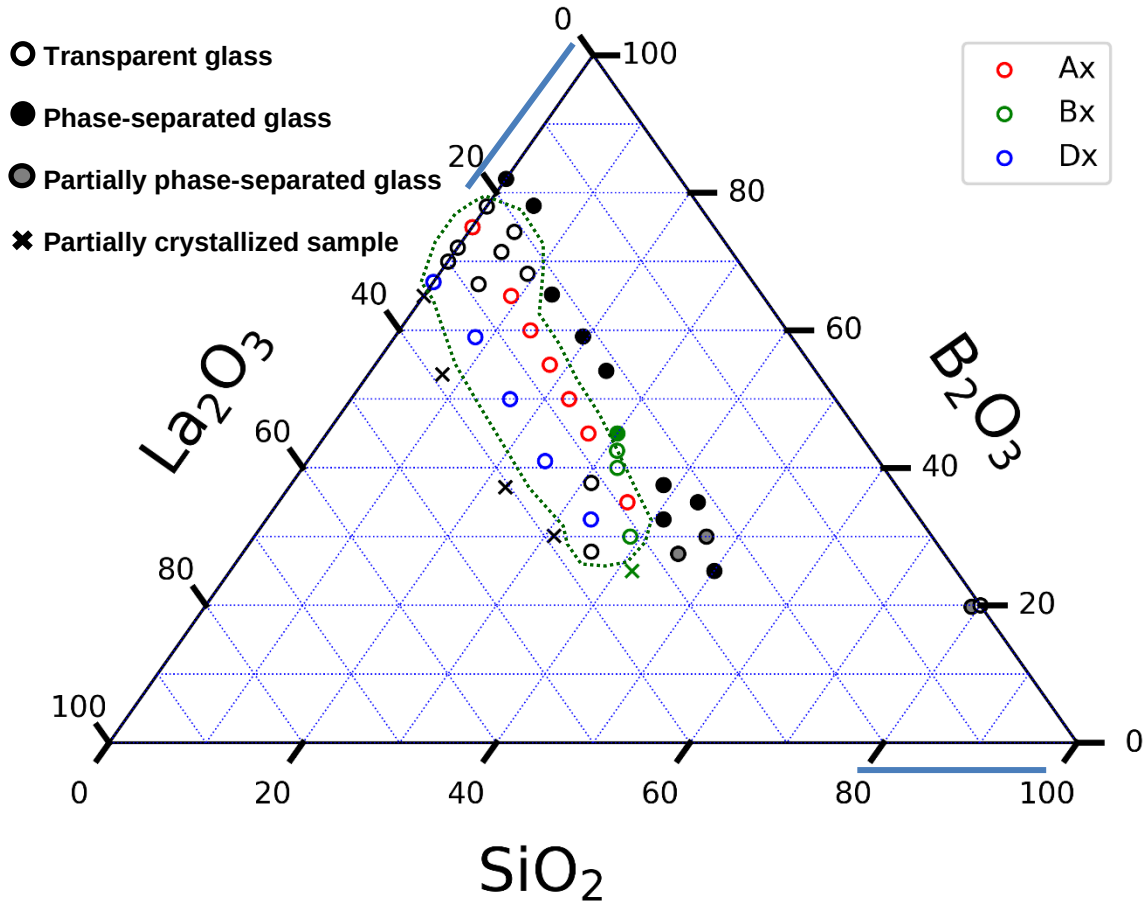
Transparent glass
Phase-separated glass
Partially phase-separated glass
Partially crystallized sample
Ax
Bx
Dx
La_2O_3
B_2O_3
SiO_2
0
20
40
60
80
100

Figure 4

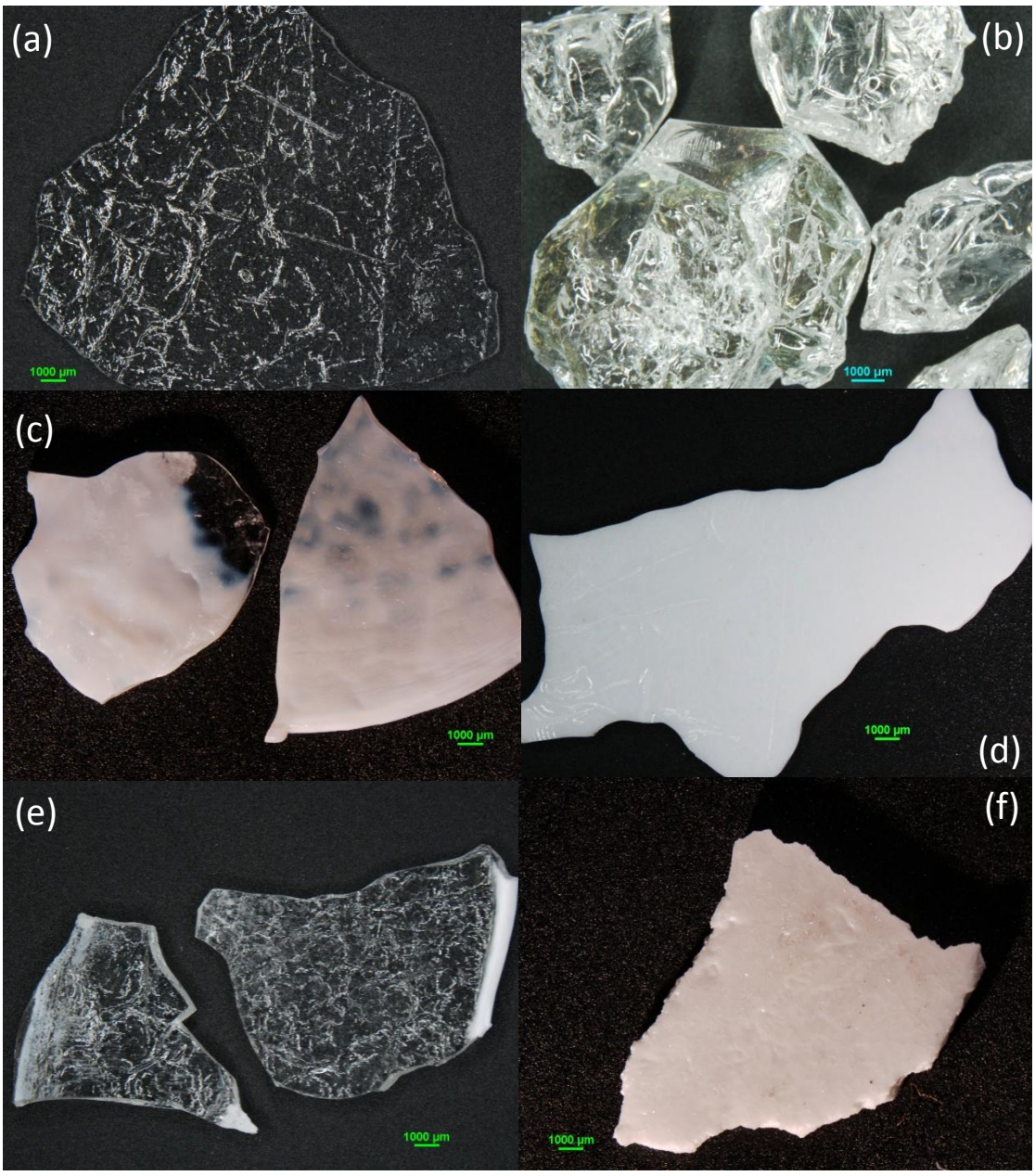

Figure 5

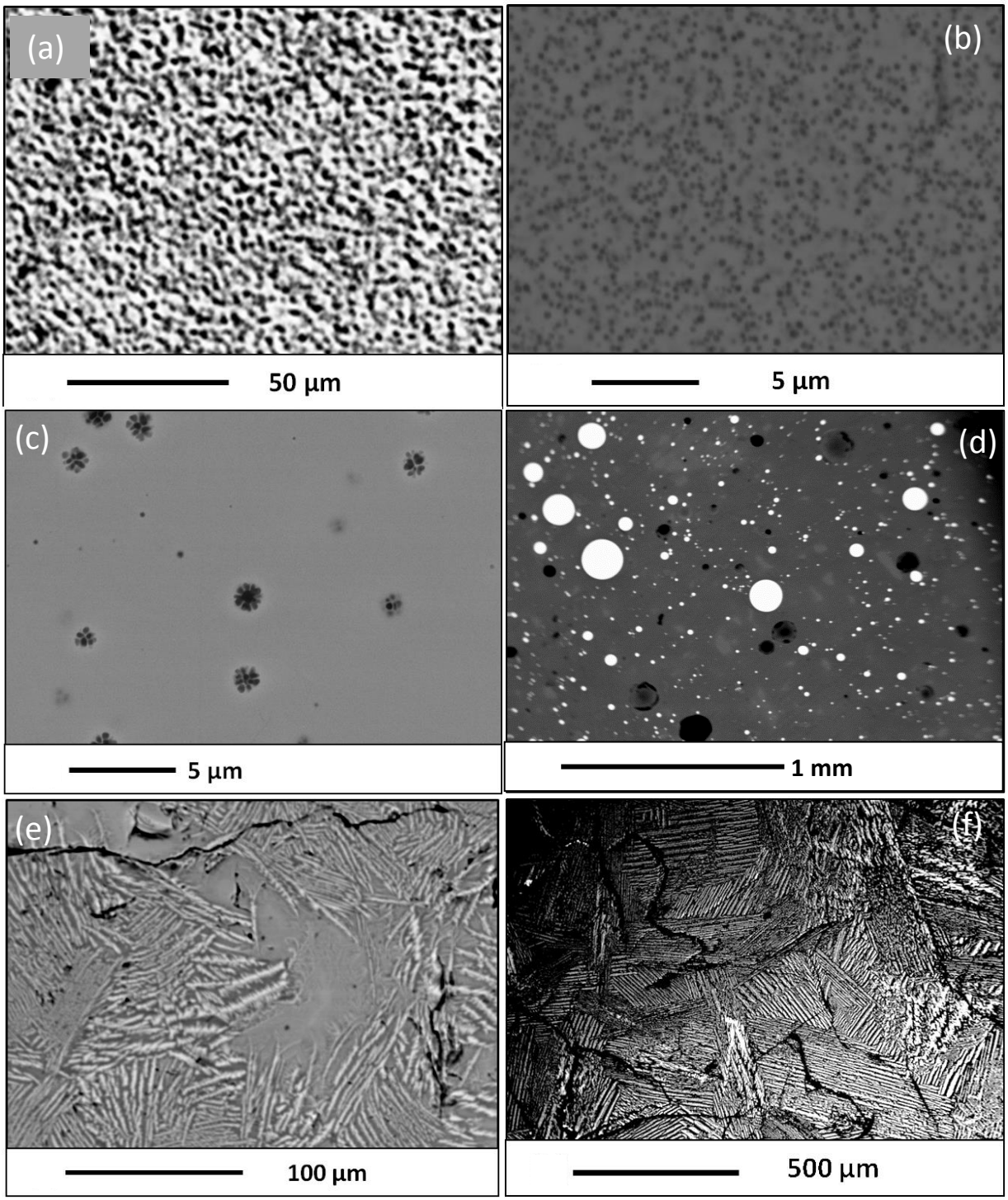

Figure 6

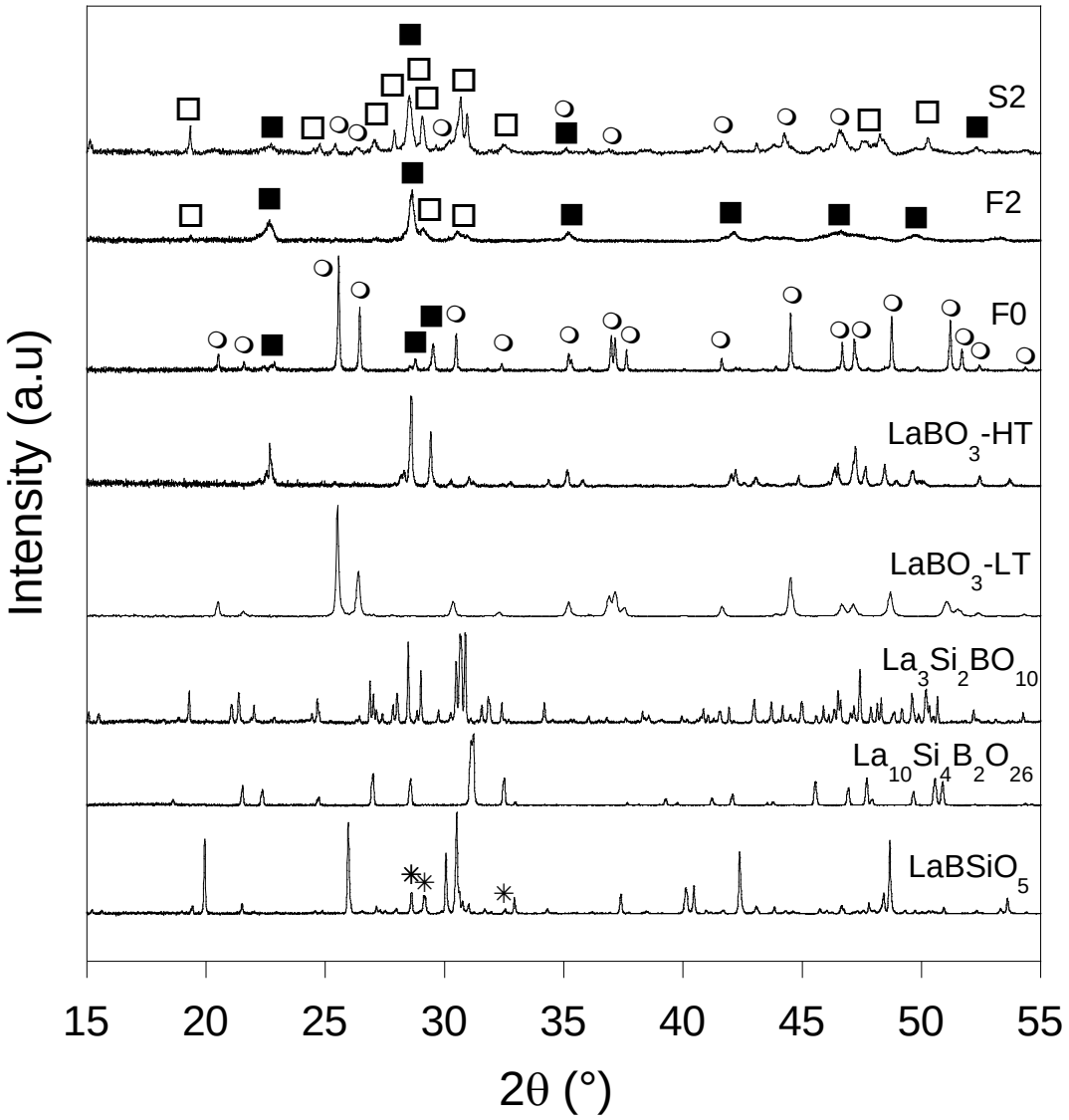
S2
F2
F0
LaBO3-HT
LaBO3-LT
La3Si2BO10
La10Si4B2O26
LaBSiO5
Intensity (a.u)
15
20
25
30
35
40
45
50
55
2θ (°)

Figure 7

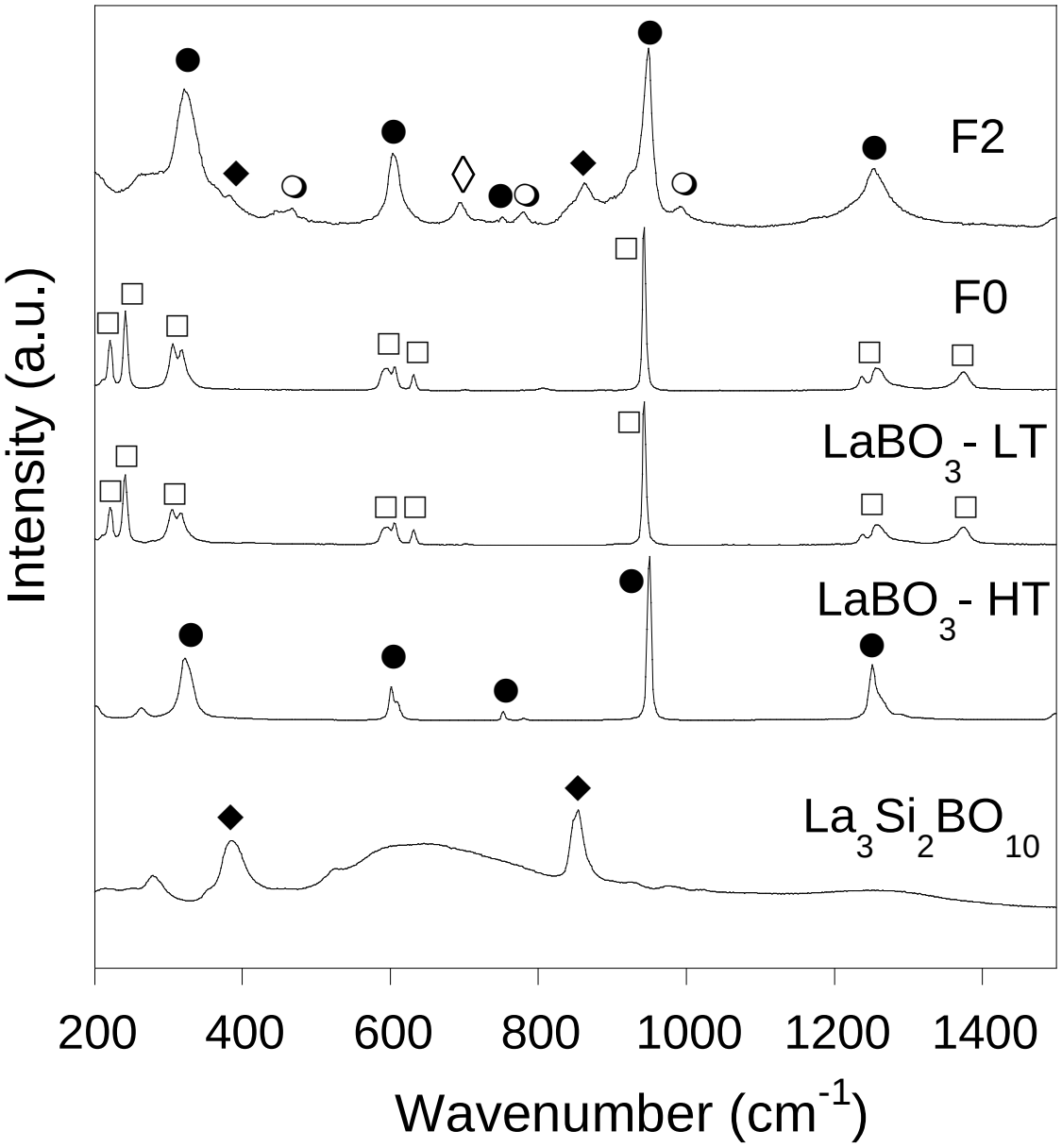
F2
F0
LaBO3 - LT
LaBO3 - HT
La3Si2BO10
Intensity (a.u.)
200
400
600
800
1000
1200
1400
Wavenumber (cm-1)

Figure 8

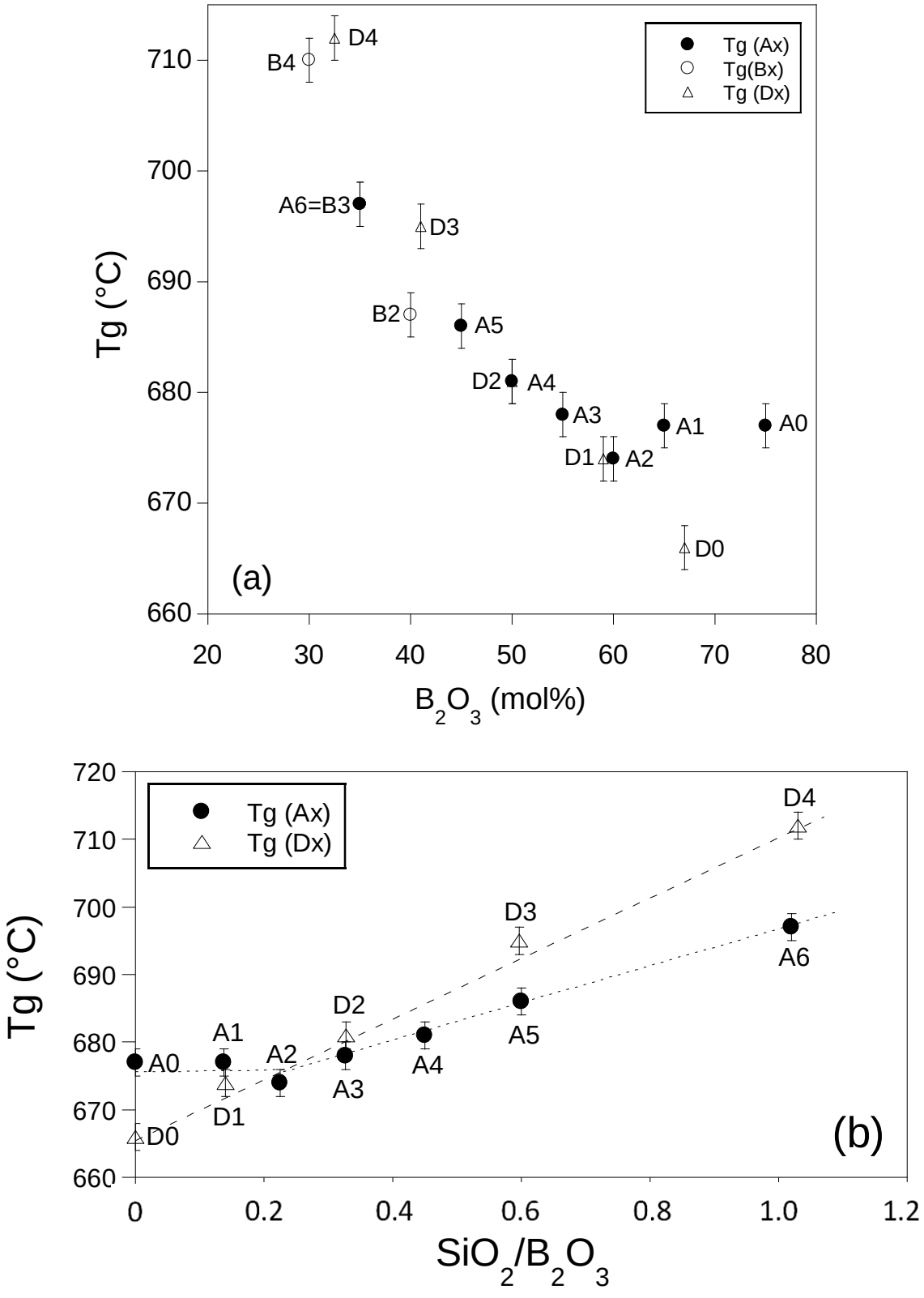
Tg (Ax)
Tg(Bx)
Tg (Dx)
B4
D4
A6=B3
D3
B2
A5
D2
A4
A3
A1
A0
D1
A2
D0
(a)
Tg (°C)
B2O3 (mol%)
Tg (Ax)
Tg (Dx)
D4
D3
A6
D2
A1
A5
A0
A2
A4
A3
D1
D0
(b)
Tg (°C)
SiO2/B2O3

Figure 9

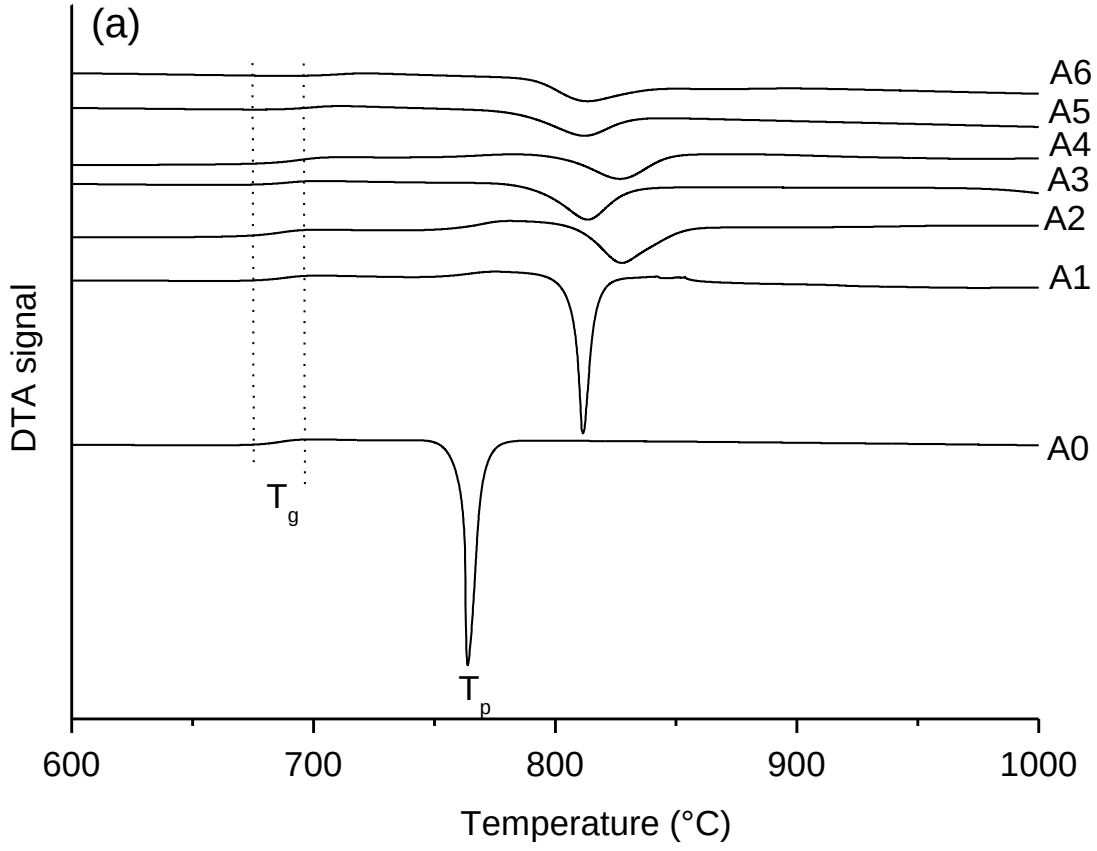
(a)
A6
A5
A4
A3
A2
A1
A0
DTA signal
T_g
T_p
600
700
800
900
1000
Temperature (°C)

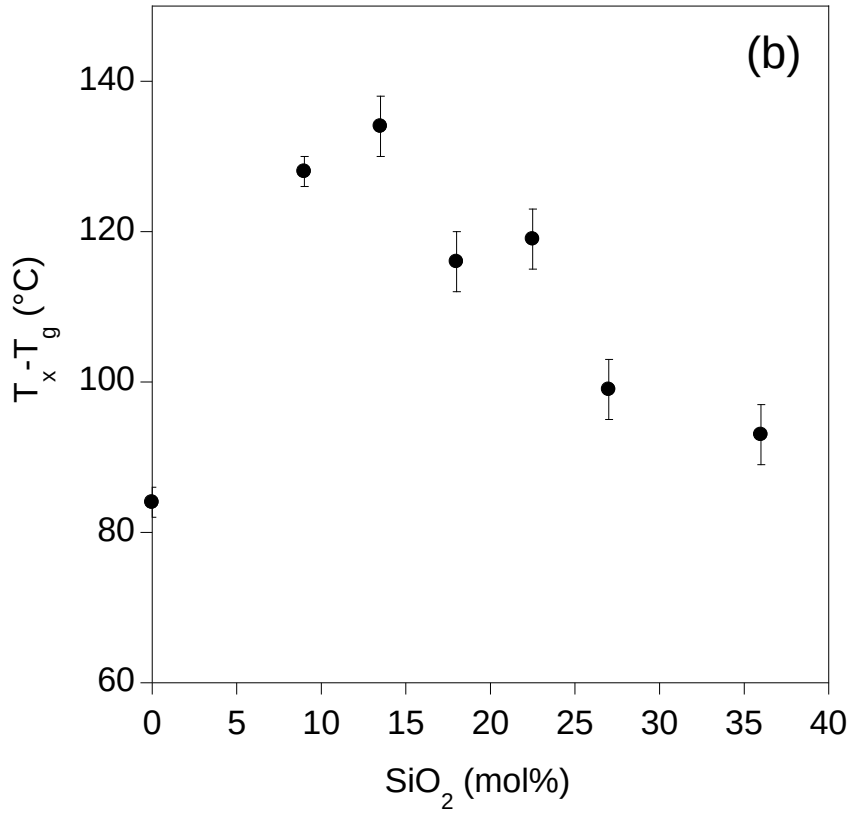
(b)
140
120
100
80
60
T_x-T_g (°C)
0
5
10
15
20
25
30
35
40
SiO_2 (mol%)

Figure 10

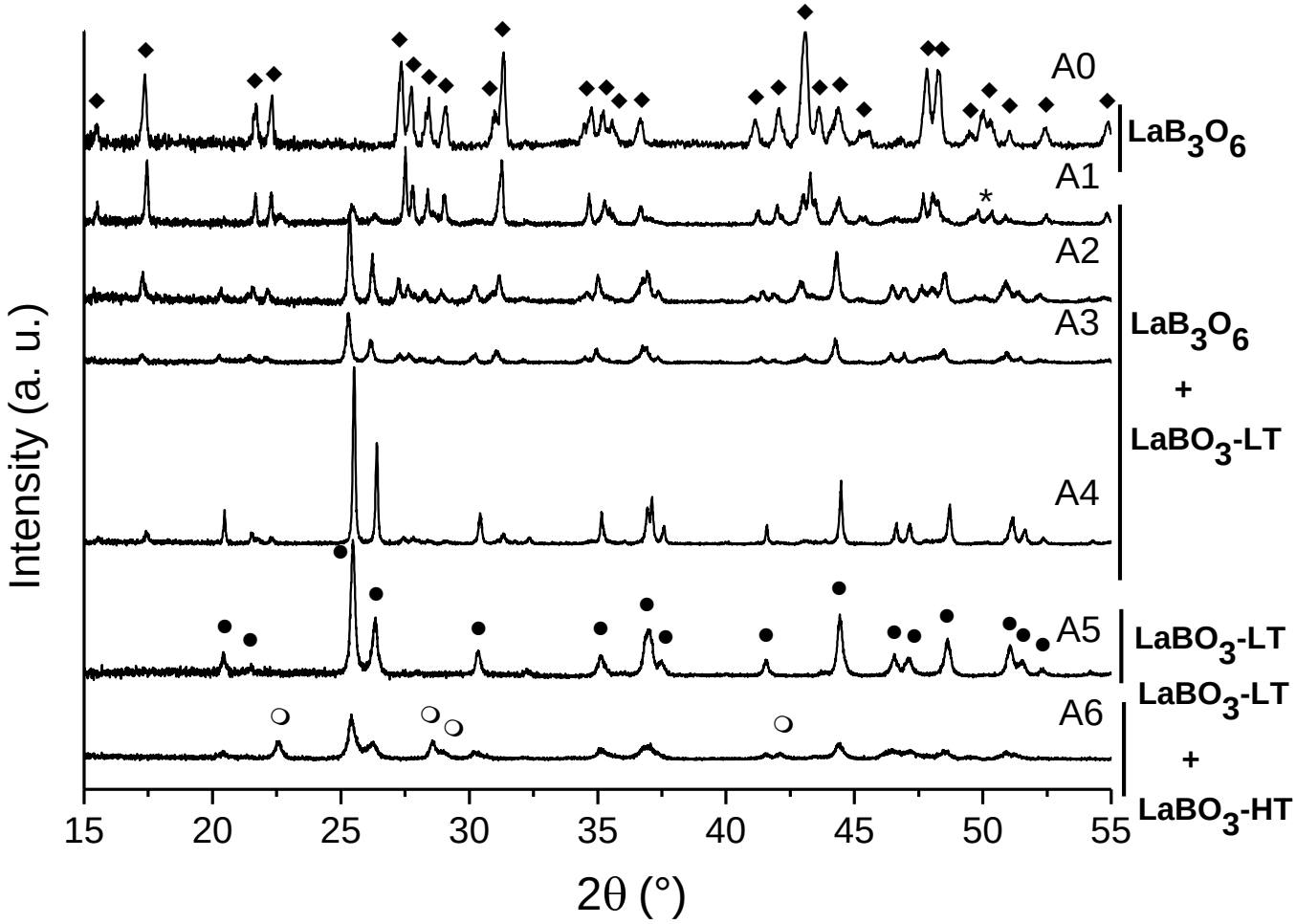
A0
A1
A2
A3
A4
A5
A6
LaB3O6
LaB3O6
+
LaBO3-LT
LaBO3-LT
LaBO3-LT
+
LaBO3-HT
Intensity (a. u.)
2θ (°)
15
20
25
30
35
40
45
50
55

Figure 11

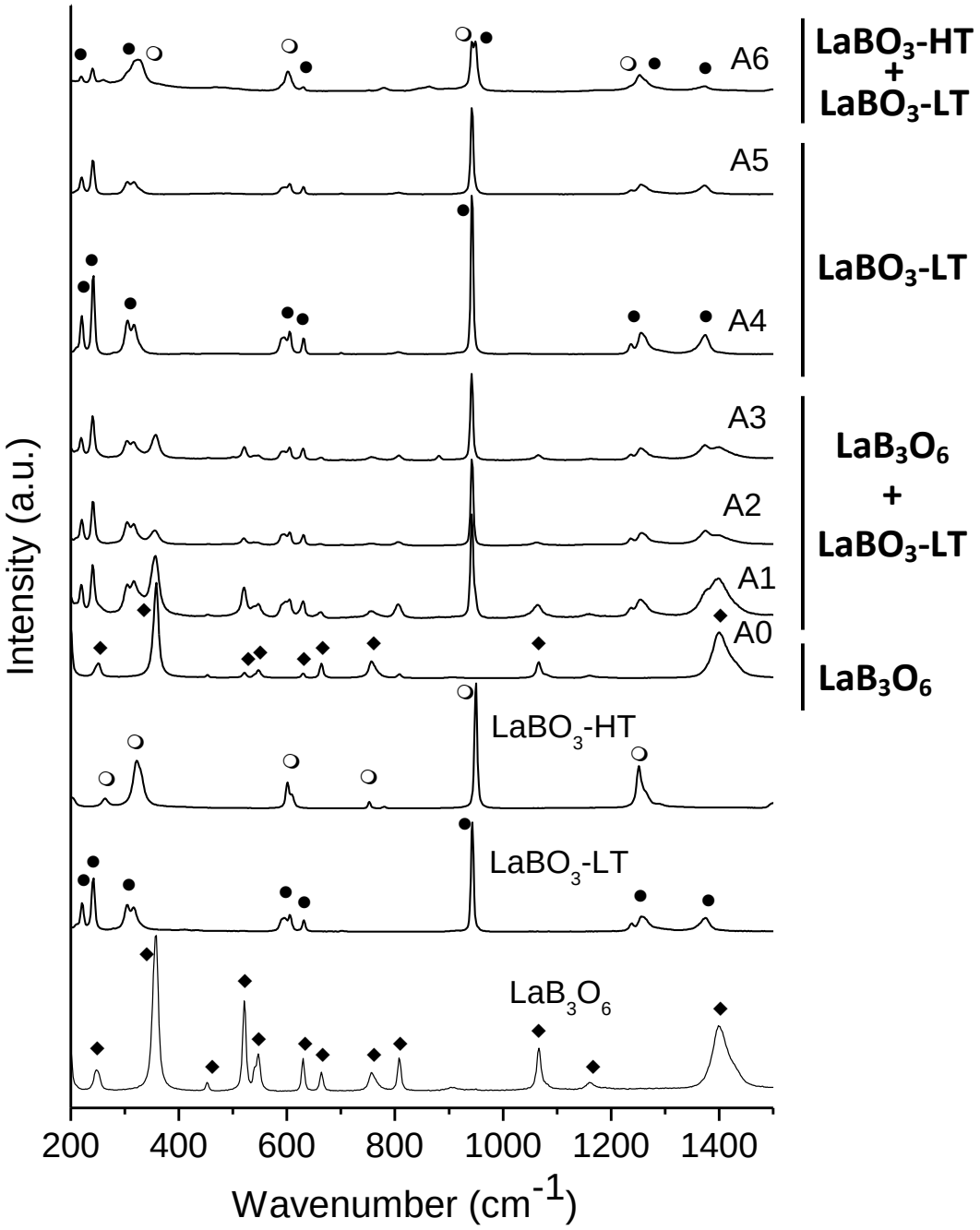
A6
A5
A4
A3
A2
A1
A0
LaBO3-HT
LaBO3-LT
LaB3O6
LaBO3-HT
+
LaBO3-LT
LaBO3-LT
LaB3O6
+
LaBO3-LT
LaB3O6
LaBO3-HT
LaBO3-LT
LaB3O6
Intensity (a.u.)
200
400
600
800
1000
1200
1400
Wavenumber (cm-1)

Figure 12

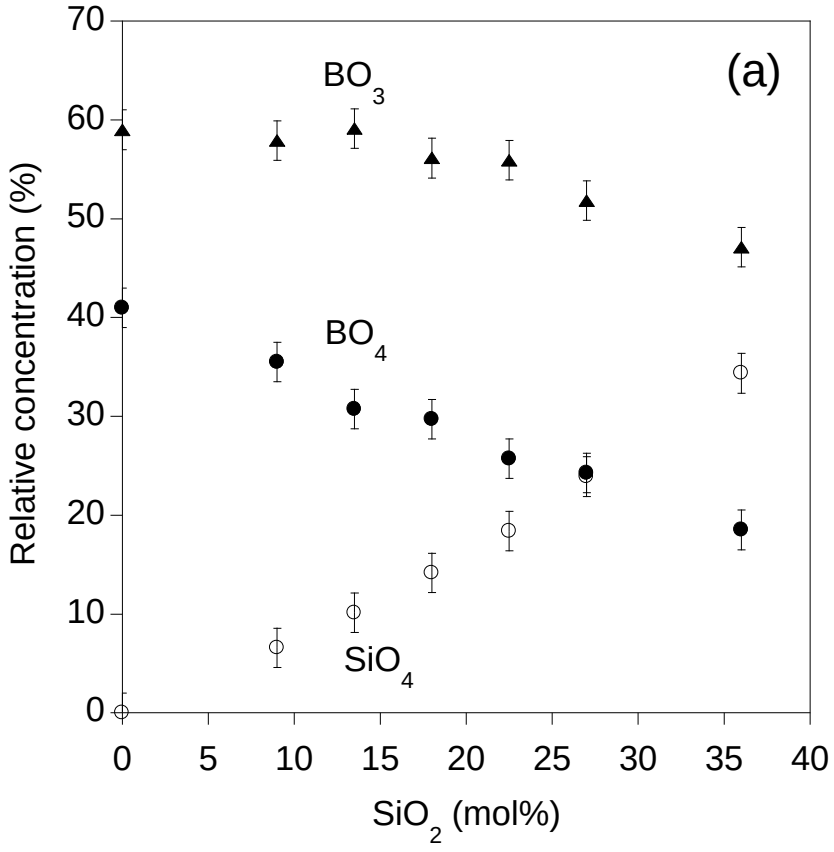
(a)
BO3
BO4
SiO4
Relative concentration (%)
SiO2 (mol%)
0
10
20
30
40
50
60
70
0
5
10
15
20
25
30
35
40

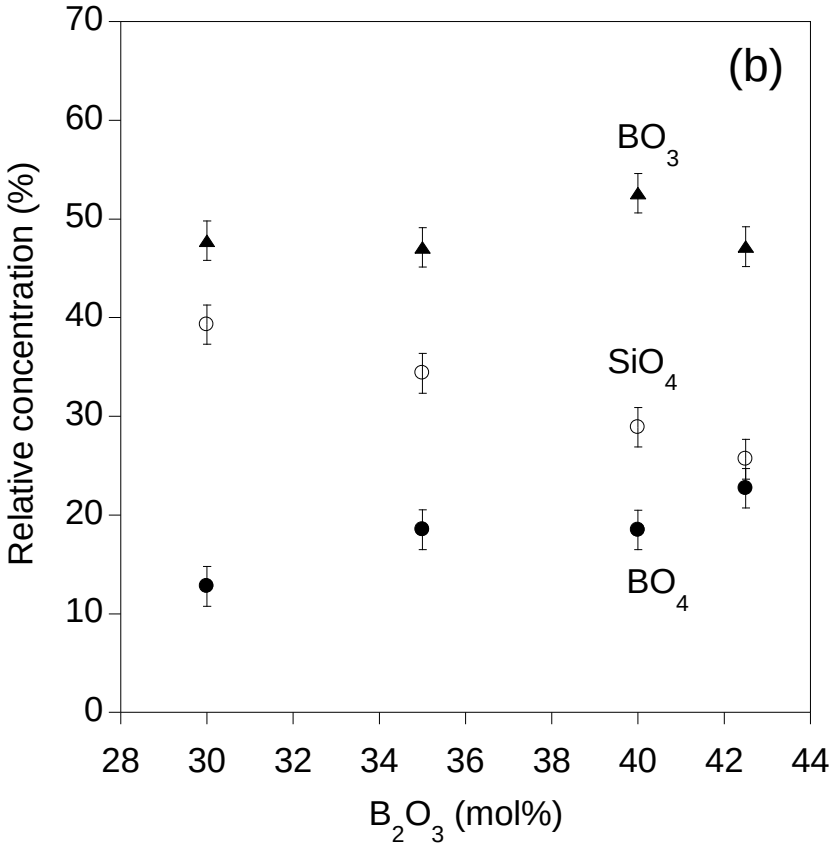
(b)
BO3
SiO4
BO4
Relative concentration (%)
B2O3 (mol%)
0
10
20
30
40
50
60
70
28
30
32
34
36
38
40
42
44

Figure 12 (continue)

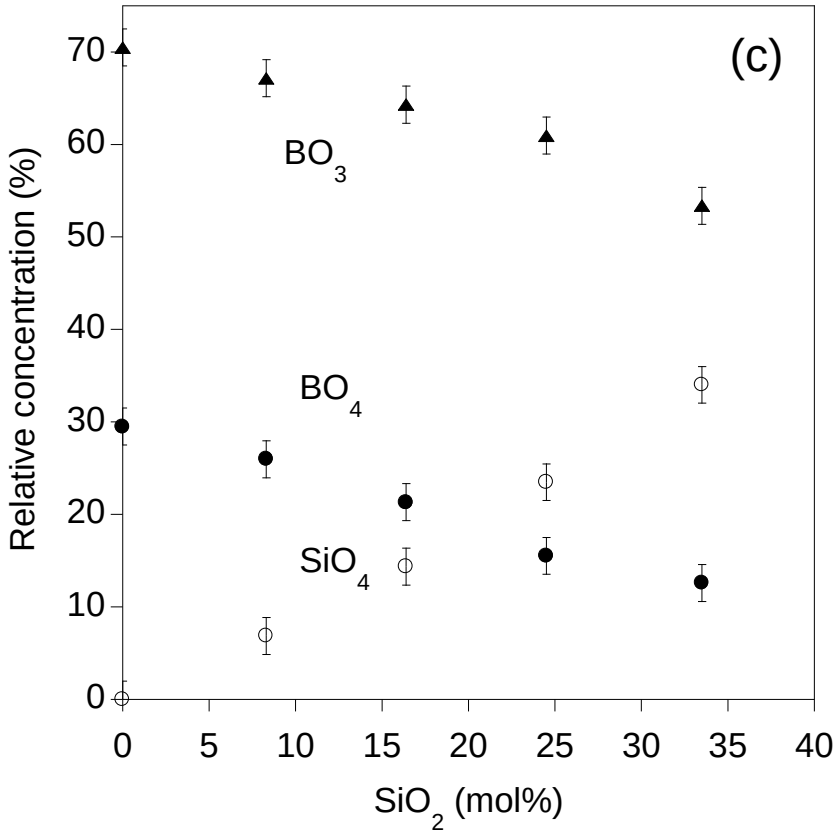

Figure 13

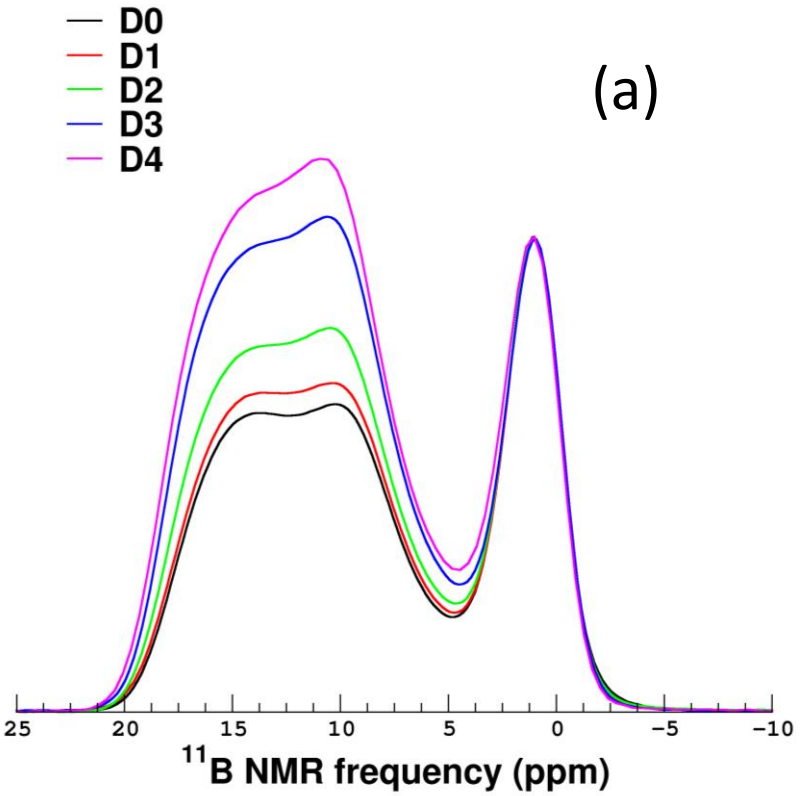
D0
D1
D2
D3
D4
(a)
25
20
15
10
5
0
−5
−10
^{11}B NMR frequency (ppm)

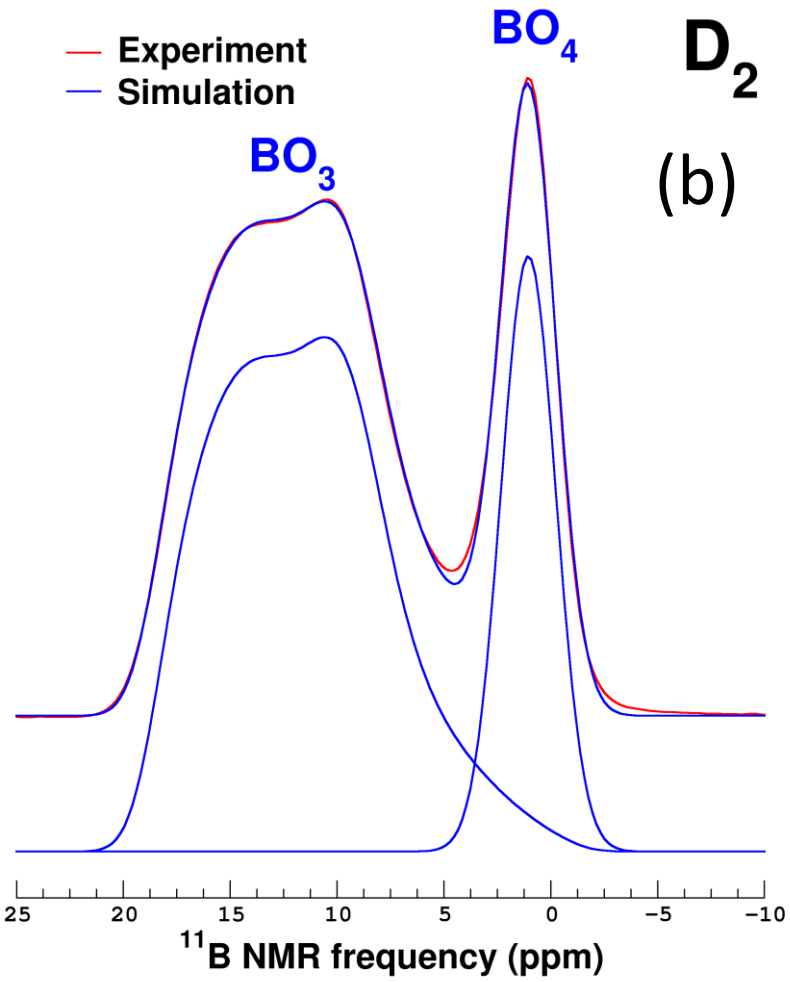
Experiment
Simulation
BO$_4$
D$_2$
BO$_3$
(b)
25
20
15
10
5
0
−5
−10
^{11}B NMR frequency (ppm)

References

[1] E. Vernaz, S. Gin, C. Veyer, "Waste glass," Comprehensive Nuclear Materials 5 (2012) 451.

[2] D. Caurant, P. Loiseau, O. Majérus, V. Aubin-Chevaldonnet, I. Bardez, A. Quintas, "Glasses, Glass-Ceramics and Ceramics for Immobilization of Highly Radioactive Nuclear Wastes," Nova Science Publishers, Hauppauge, New York, 2009.

[3] O. Majérus, D. Caurant, A. Quintas, J.L. Dussossoy, I. Bardez, P. Loiseau, "Effect of boron oxide addition on the Nd^{3+} environment in a Nd-rich soda-lime aluminoborosilicate glass," J. Non-Cryst. Solids 357 (2011) 2744.

[4] H. Li, Y. Su, L. Li, D.M. Strachan, "Raman spectroscopic study of gadolinium (III) in sodium-aluminoborosilicate glasses," J. Non-Cryst. Solids 292 (2001) 167.

[5] L. Li, H. Li, M. Qian, D.M Strachan, "Gadolinium solubility in peralkaline borosilicate glasses," J. Non-Cryst. Solids 283 (2001) 237.

[6] H. Li, L. Li, J. D. Vienna, M. Qian, Z. Wang, J.G. Darab, D.K. Peeler, "Neodymium (III) in alumino-borosilicate glasses," J. Non-Cryst. Solids 278 (2001) 35.

[7] I. Chakraborty, J. Shelby, R. Condrate, "Properties and structure of lanthanum borate glasses," J. Am. Ceram. Soc. 67 (1984) 782.

[8] K. Terashima, S. Tamura, S-H. Kim, T. Yoko, "Structure and nonlinear optical properties of lanthanide borate glasses," J. Am. Ceram. Soc. 80 (1997) 2903.

[9] H. Trégouët, D. Caurant, O. Majérus, T. Charpentier, L. Cormier, D.S. Pytalev, "Spectroscopic investigation and crystallization study of rare earth metaborate glasses," Procedia Mater. Sci. 7 (2014) 131.

[10] D.S. Pytalev, D. Caurant, O. Majérus, H. Trégouët, T. Charpentier, B.N. Mavrin, "Structure and crystallization behavior of $La_2O_3 \cdot 3B_2O_3$ metaborate glasses doped with Nd^{3+} or Eu^{3+} ions," J. Alloys Compd. 641 (2015) 43.

[11] V.N. Sigaev, A.V. Dechev, S.L. Kadyshman, O.L. Al'takh, S.Yu. Stefanovich, V.I. Molev, "Glasses of the system La_2O_3-B_2O_3-SiO_2 and crystallization of the ferroelectric phase $LaBSiO_5$," Glass Phys. Chem. 22 (1996) 3.

[12] I.A. Levitskii, M.V. Dyadenko, L.F. Papko, "BaO-La_2O_3-B_2O_3-TiO_2-SiO_2 glass production," Glass Ceram. 68 (2012) 315.

[13] J.T. Sun, J.H. Zhang, B.J. Chen, S.Z. Lu, X.G. Ren, X.J. Wang, "Preparation and optical properties of Er^{3+}-doped gadolinium borosilicate glasses," J. Rare Earths 23 (2005) 157.

[14] F. Angeli, T. Charpentier, E. Molières, A. Soleilhavoup, P. Jollivet, S. Gin, "Influence of lanthanum on borosilicate glass structure: A multinuclear MAS and MQMAS NMR investigation," J. Non-Cryst. Solids 376 (2013) 189.

[15] J.E. Shelby, "Rare earths as major components in oxide glasses," Key Engineering Materials, Trans Tech Publications (Ed. by J.E. Shelby) 94-95 (1994) 1.

[16] J.T. Kohli, J.E. Shelby, "Formation and properties of rare earth aluminosilicate glasses," Phys. Chem. Glasses 32 (1991) 67.

[17] J.E. Shelby, J.T. Kohli, "Rare-earth aluminosilicate glasses," J. Am. Ceram. Soc. 73 (1990) 39.

[18] T. Schaller, J.F. Stebbins, "The structural role of lanthanum and yttrium in aluminosilicate glasses: a ^{27}Al and ^{17}O MAS NMR study," J. Phys. Chem. B 102 (1998) 10690.

[19] N.J. Clayden, S. Esposito, A. Aronne, P. Pernice, "Solid state ^{27}Al NMR and FTIR study of lanthanum aluminosilicate glasses," J. Non-Cryst. Solids 258 (1999) 11.

[20] N. Sadiki, J.P. Coutures, C. Fillet, J.L. Dussossoy, "Crystallization of lanthanum and yttrium aluminosilicate glasses," J. Nucl. Mater. 348 (2006) 70.

[21] S. Gavarini, F. Carrot, G. Matzen, P. Trocellier, “Dissolution of LnYSiAlO glass (Ln=La or Ce) in aqueous media. I. Influence of the pH on hydrolysis mechanisms and kinetics,” J. Non-Cryst. Solids 332 (2003) 115.

[22] S. Iftekhar, J. Grins, P.N. Gunawidjaja, M. Edén, “Glass formation and structure–property-composition relations of the RE_2O_3–Al_2O_3–SiO_2 (RE=La, Y, Lu, Sc) systems,” J. Am. Ceram. Soc. 94 (2011) 2429.

[23] A. Jaworski, B. Stevenson, M. Edén, “The bearings from rare-earth (RE = La, Lu, Sc, Y) cations on the oxygen environments in aluminosilicate glasses: A study by solid-state ^{17}O NMR, molecular dynamics simulations, and DFT calculations,” J. Phys. Chem. C 120 (2016) 13

[24] O. Majérus, H. Trégouët, D. Caurant, D. Pytalev, “Comparative study of the rare earth environment in rare earth metaborate glass (REB_3O_6, RE = La, Nd) and in sodium borate glasses,” J. Non-Cryst. Solids 425 (2015) 91.

[25] E. Levin, C. Robbins, J. Waring, “Immiscibility and the system lanthanum oxide-boric oxide,” J. Am. Ceram. Soc. 44 (1961) 87−91.

[26] N.A. Toropov, I.A. Bondar, “New silicates in the system La_2O_3-SiO_2,” Bull. Acad. Sci. USSR, Div. Chem. Sci. 10 (1961) 682.

[27] J. Felsche, “Rare earth silicates with the apatite structure,” J. Solid State Chem. 5 (1972) 266.

[28] J. Felsche, “The crystal chemistry of the rare-earth silicates,” in Structure and Bonding 13 (1973) 99.

[29] T.J. Rockett, W.R. Foster, “Phase relations in the system boron oxide-silica,” J. Am. Ceram. Soc. 48 (1965) 75.

[30] E.M. Levin, R.S. Roth, J.B. Martin, “Polymorphysm of ABO_3 type rare earth borates,” Am. Mineral. 46 (1961) 1030.

[31] A. Nakatsuka, O.Ohtaka, H. Arima, N. Nakayama, T. Mizota, "Aragonite-type lanthanum orthoborate, $LaBO_3$," Acta Cryst. E 62 (2006) i103.

[32] S. Lemanceau, G. Bertrand-Chadeyron, R. Mahiou, M. El-Ghozzi, J.C. Cousseins, P. Conflant, R.N. Vannier, "Synthesis and characterization of H-$LnBO_3$ orthoborates (Ln = La, Nd, Sm, and Eu)," J. Solid State Chem. 148 (1999) 229.

[33] J. McAndrew, T.R. Scott, "Stillwellite, a new rare-earth mineral from Queensland," Nature 176 (1955) 509.

[34] I.I. Nekrasov, R.A. Nekrasova, "Conditions of formation of synthetic analogs of stillwellite $LnBO[SiO_4]$," Dokl. Akad. Nauk SSSR 201 (1971) 1202.

[35] H.K. Juwhari, W.B. White, "Luminescence of rare earth borosilicates with the stillwellite and related structures," Mater. Lett. 64 (2010) 1751.

[36] A.A. Voronkov, Y.A. Pyatenko, "X-ray diffraction study of the atomic structure of stillwellite $CeBO[SiO_4]$," Sov. Phys. Crystallogr. USSR 12 (1967) 214.

[37] P.C. Burns, F. C. Hawthorne, D.J. MacDonald, G.D. Ventura, G.C. Parodi, "The crystal structure of stillwellite," Can. Mineral. 31 (1993) 147.

[38] L. Chi, H. Chen, H. Zhuang, J. Huang, "Crystal structure of $LaBSiO_5$," J. Alloy. Compd. 252 (1997) L12.

[39] J.S. Ysker, W. Hoffmann, "Die Kristallstruktur des $La[B_3O_6]$," Naturwissenschaften 57 (1970) 129.

[40] Y. Ono, K. Takayama, T. Kajitani, "X-ray diffraction study of $LaBSiO_5$," J. Phys. Soc. Jpn. 65 (1996) 3224.

[41] B.A. Strukov, E.P. Ragula, S.Yu. Stefanovich, I.V. Shnaidshtein, S.V. Arkhangel'skaya, A. Onodera, "Ferroelectric phase transition in $LaBSiO_5$ crystals from results of thermal and dielectric measurements," Phys. Sol. State 40 (1998) 1193.

[42] S.Yu. Stefanovich, V.N. Sigaev, A.V. Dechev, A.V. Mosunov, V.R. Samygina, N.I. Leonyuk, P.D. Sarkisov, "Ferroelectric Properties of $LNBSiO_5$ (LN=La, Pr) borosilicates, analog of stilwellite," Neorgan Mater. 31 (1995) 756.

[43] N.I. Leonyuk, E.L. Belokoneva, G. Bocelli, L. Righi, E.V. Shvanskii, R.V. Henrykhson, N.V. Kulman, D.E. Kozhbakhteeva, "High-temperature crystallization and X-ray characterization of Y_2SiO_5, $Y_2Si_2O_7$ and $LaBSiO_5$," J. Cryst. Growth 205 (1999) 361.

[44] D. Savage, J.E. Robbins, R.J. Merriman, "Hydrothermal crystallization of a radioactive waste storage glass," Mineral. Mag. 49 (1985) 195.

[45] A. Rulmont, P. Tarte, "Lanthanide borogermanates $LnBGeO_5$: synthesis and structural study by X-ray diffractometry and vibrational spectroscopy," J. Solid State Chem. 75 (1988) 244.

[46] K. Serhan, M. Taïbi, J. Aride, A. Boukhari, J. Darriet, G. Le Flem, "The crystal structure of a new borogermanosilicate $Nd_3BGe_{1.08}Si_{0.92}O_{10}$," J. Solid State Chem. 110 (1994) 384.

[47] L. Chi, H. Chen, S. Deng, H. Zhuang, J. Huang, "Synthesis and crystal structure of a new samarium borosilicate compound $Sm_3BSi_2O_{10}$," J. Alloys Compd. 242 (1996) 1.

[48] L. Chi, H. Chen, S. Deng, H. Zhuang, J. Huang, "A new europium borosilicate, $Eu_3BSi_2O_{10}$," Acta Cryst. Sect. C 109 (1996) 1049.

[49] H. Müller-Bunz, H. Grossholz, T. Schleid, "Einkristalle des Cer(III)-Borosilicats $Ce_3[BSiO_6][SiO_4]$," Z. Anorg. Allg. Chem. 627 (2001) 1436.

[50] H. Müller-Bunz, T. Schleid, "$Nd_3BSi_2O_{10}$: Ein neuartiges Borosilicat des Neodyms gemäß $Nd_3[BSiO_6][SiO_4]$", Z. Kristallogr. Suppl. 15 (1998) 48.

[51] E.V. Shvanskii, N.I. Leonyuk, G. Bocelli, L. Righi, "Crystallization and structural characteristics of new borosilicates," J. Solid State Chem. 154, (2000) 312.

[52] E. Gasnier, I. Bardez-Giboire, V. Montouillout, N. Pellerin, M. Allix, N. Massoni, S. Ory, M. Cabie, S. Poissonnet, D. Massiot, "Homogeneity of peraluminous SiO_2–B_2O_3–Al_2O_3–Na_2O–CaO–Nd_2O_3 glasses: Effect of neodymium content," J. Non-Cryst. Solids 405 (2014) 55.

[53] D. Mazza, M. Tribaudino, A. Delmastro, B. Lebech, "Synthesis and neutron diffraction study of $La_5Si_2BO_{13}$, an analog of the apatite mineral," J. Solid State Chem. 155 (2000) 389.

[54] J-L. Yuan, Z-J. Zhang, X-J. Wang, H-H. Chen, J-T. Zhao, G-B. Zhang, C-S. Shi, "Synthesis and VUV–UV spectroscopic properties of rare earth borosilicate oxyapatite: $RE_5Si_2BO_{13}$:Ln^{3+} (RE=La, Gd, Y; Ln=Eu, Tb)," J. Solid State Chem. 180 (2007) 1365.

[55] S.A. Naidu, U.V. Varadaraju, B. Raveau, "Eu^{3+} luminescence in $La_5Si_2BO_{13}$ with apatite related structure and magnetic studies in $Ln_5Si_2BO_{13}$ (Ln = Gd, Dy)," J. Solid State Chem. 183 (2010) 1847.

[56] P. Chen, R.K. Li, "Two high terbium content apatites: $Tb_5Si_2BO_{13}$ and $Tb_{4.66}Si_3O_{13}$," J. Alloys Compd. 622 (2015) 859.

[57] H. Xu, Z. Xia, H. Liu, L. Liao, "Luminescence properties and energy transfer in $La_{5-x-y}Si_2BO_{13}$:xCe^{3+}, yTb^{3+} phosphor," ECS J. Solid State Sci. Technol. **2** (2013) R186.

[58] V.N. Sigaev, E.V. Lopatina, P.D. Sarkisov, S.Y. Stefanovich, V. I. Molev, "Grain-oriented surface crystallization of lanthanum borosilicate and lanthanum borogermanate glasses," Mater. Sci. Eng. B 48 (1997) 254.

[59] I. Kratochvílová-Hrubá, I. Gregora, J. Pokorný, S. Kamba, Z. Zikmund, J. Petzelt, M. Čerňanský, V. Studnička, V.N Sigaev, E.N. Smelyanskaya, "Vibrational spectroscopy of $LaBSiO_5$ glass and glass-crystal composites," J. Non-Cryst. Solids 290 (2001) 224.

[60] G.A. Komandin, "Electrodynamic characteristics of the $LaBGeO_5$ and $LaBSiO_5$ glasses in the terahertz and infrared ranges," Phys. Solid State 54 (2012) 2189.

[61] V.N. Sigaev, S.Y. Stefanovich, P.D. Sarkisov, E.V. Lopatina, "Stillwellite glass-ceramics with ferroelectric properties," Mater. Sci. Eng. B 32 (1995) 17.

[62] P. Gupta, H. Jain, D.B. Williams, O. Kanert, R. Kuechler, "Structural evolution of $LaBGeO_5$ transparent ferroelectric nano-composites," J. Non-Cryst. Solids 349 (2004) 291.

[63] V.N. Sigaev, S.V. Lotarev, E.V. Orlova, S.Yu. Stefanovich, P. Pernice, A. Aronne, E. Fanelli, I. Gregora, "Lanthanum borogermanate glass-based active dielectrics," J. Non-Cryst. Solids 353 (2007) 1956.

[64] M. Magnin, S. Schuller, C. Mercier, J. Trébosc, D. Caurant, O. Majérus, F. Angéli, T. Charpentier, "Modification of molybdenum structural environment in borosilicate glasses with increasing content of boron and calcium oxide by ^{95}Mo MAS NMR," J. Am. Ceram. Soc. 94 (2011) 4274.

[65] T. Charpentier, C. Fermon, J. Virlet, "Numerical and theoretical analysis of multiquantum magic-angle spinning experiments," J. Chem. Phys. 109 (1998) 3116.

[66] Handbook of Chemistry and Physics, D. R. Lide ed., CRC Press, 84th edition, 2003-2004.

[67] S. K. Lee, J. F. Steebins, "Extent of intermixing among framework units in silicate glasses and melts," Geochim. Cosmochim. Acta 66 (2002) 303.

[68] A. Soleilhavoup, J-M. Delaye, F. Angeli, D. Caurant, T. Charpentier, "Contribution of first-principles calculations to multinuclear NMR analysis of borosilicate glasses," Magn. Reson. Chem. 48 S1 (2010) S159.

[69] R.J. Charles, F.E. Wagstaff, "Metastable immiscibility in the B_2O_3-SiO_2 system," J. Am. Ceram. Soc. 51 (1968) 16.

[70] A.C. Vaz de Araújo, I.T. Weber, B.S. Santos, B.J.P. da Silva, R.P. de Mello Jr., S. Alves Jr., G.F. de Sá, C. de Mello Donegá, "Spectroscopy and crystallization behavior of Eu^{3+}-doped La_2O_3:B_2O_3 binary glasses," J. Non-Cryst. Solids 219 (1997) 160.

[71] A. Marotta, V.N. Sigaev, E.V. Lopatina, "Non-isothermal crystallization of lanthanum-borate glasses," J. Mater. Sci. Lett. 15 (1996) 145.

[72] Yu.K. Voron'ko, L.N. Galaktionov, L.N. Dmitruk, O.B. Petrova, A.V. Popov, S.N. Ushakov, Vl.E. Shukshin, "Spectroscopic studies of glasses based on rare-earth borates," Glass Phys. Chem. 32 (2006) 47.

[73] N.N. Vinogradova, L.N. Dmitruk, O.B. Petrova, "Glass transition and crystallization of glasses based on rare-earth borates," Glass Phys. Chem. 33 (2004) 1.

[74] E.M. Levin, C.R. Robbins, J.L. Waring, "Immiscibility and the system lanthanum oxide-boric oxide," J. Am. Ceram. Soc. 44 (1961) 87.

[75] H. Trégouët, "Structure et cristallisation de verres d'oxydes simples riches en bore et en terres rares," PhD. Thesis of the University P. and M. Curie (2016, Paris, France), www.theses.fr/2016PA066032.pdf

[76] A. Kajinami, M. Nakamura, S. Deki, "Composition dependence of local structure in lanthanoborate glasses," J. Alloys Compd. 408-412 (2006) 1238.

[77] M. Edén, "NMR studies of oxide-based glasses," Annu. Rep. Prog. Chem., Sect. C: Phys. Chem. 108 (2012) 177.

[78] N.H. Ray, "Composition-property relationships in inorganic oxide glasses," J. Non-Cryst. Solids 15 (1974) 423.

[79] R. Boekenhauer, H. Zhang, S. Feller, D. Bain, S. Kambeyanda, K. Budhwani, P. Pandikuthira, F. Alamgir, A.M. Peters, S. Messer, K.L. Loh, "The glass transition temperature of lithium borosilicate glasses related to atomic arrangements," J. Non-Cryst. Solids 175 (1994) 137.

[80] V.V. Golubkov, P.A. Onushchenko, "Temperature dependences of density of sodium borosilicate glasses in equilibrium states at temperatures below a vitrification temperature," Glass Phys. Chem. 39 (2013) 11.

[81] L. Cormier, O. Majérus, D.R. Neuville, G. Calas, "Temperature-induced structural modifications between alkali borate glasses and melts," J. Am. Ceram. Soc. 89 (2006) 13.

[82] B.A. Maksimov, E.A. Genkina, V.R. Samygina, N.I. Leonyuk, “Crystal structure of La-analog of stillwellite,” Kristallografiya 38 (1993) 61.

[83] V.A. Shuvaeva, E.L. Belokoneva, N.I. Leonyuk, M.Yu. Antipin, “Crystal structure of a high-temperature modification of $LaBSiO_5$, a synthetic analog of stillwellite,” Zh. Neorg. Khim. 41 (1996) 1097.

[84] S. Guillot, S. Beaudet-Savignat, S. Lambert, P. Roussel, G. Tricot, R.-N. Vannier, A. Rubbens, “Local relaxation in lanthanum silicate oxyapatites by Raman scattering and MAS-NMR,” J. Raman Spectrosc. 42 (2011) 1455.